

Superconductivity of LaH₁₀ and LaH₁₆: new twists of the story

Ivan A. Kruglov,^{1,2,*} Dmitrii V. Semenov,^{1,3} Hao Song⁹, Radosław Szczęśniak,^{4,5} Izabela A. Wrona,⁴ Ryosuke Akashi,⁶ M. Mahdi Davari Esfahani,⁷ Defang Duan,⁹ Tian Cui,⁹ Alexander G. Kvashnin^{3,1} and Artem R. Oganov^{3,2,8}

¹ Moscow Institute of Physics and Technology, 9 Institutsky lane, Dolgoprudny 141700, Russia

² Dukhov Research Institute of Automatics (VNIIA), Moscow 127055, Russia

³ Skolkovo Institute of Science and Technology, Skolkovo Innovation Center, 3 Nobel Street, Moscow 121205, Russia

⁴ Institute of Physics, Jan Dlugosz University in Czestochowa, Ave. Armii Krajowej 13/15, 42-200 Czestochowa, Poland

⁵ Institute of Physics, Czestochowa University of Technology, Ave. Armii Krajowej 19, 42-200 Czestochowa, Poland

⁶ University of Tokyo, 7-3-1 Hongo, Bunkyo, Tokyo 113-8654, Japan

⁷ Department of Geosciences and Center for Materials by Design, Institute for Advanced Computational Science, State University of New York, Stony Brook, NY 11794-2100, USA

⁸ International Center for Materials Discovery, Northwestern Polytechnical University, Xi'an, 710072, China

⁹ Key State Laboratory of Superhard Materials, Jilin University, Changchun, China

Corresponding Authors

*Ivan A. Kruglov, E-mail: ivan.kruglov@phystech.edu

*Dmitrii V. Semenov, E-mail: dmitrii.semenov@skoltech.ru

*Artem R. Oganov, E-mail: a.oganov@skoltech.ru

ABSTRACT. Recent experiments have established previously predicted LaH₁₀ as the highest-temperature superconductor, with T_C up to 250-260 K [1]. In this work we explore the high-pressure phase stability and superconductivity of lanthanum hydrides LaH_{*m*}. We predict the stability of a hitherto unreported polyhydride *P* 6/*mmm*-LaH₁₆ at pressures above 150 GPa; at 200 GPa its predicted superconducting T_C is 156 K, critical field $\mu_0 H_C(0) \sim 35$ T and superconducting gap is up to 35 meV. We revisit the superconductivity of LaH₁₀ and find its T_C to be up to 259 K at 170 GPa from solving the Eliashberg equation and 271 K from solving the gap equation in SCDF, which also allowed us to compute the Coulomb pseudopotential μ^* for LaH₁₀ and LaH₁₆. The presence of several polymorphic modifications of LaH₁₀ may explain the variety in its measured T_C values [1,2].

Introduction

Recently, superhydrides of various elements attracted a great attention: they were first predicted and then experimentally proven to exhibit a record high-temperature superconductivity under a high pressure. According to the Bardeen-Cooper-Schrieffer (BCS) theory, the metallic hydrogen is expected to be a high- T_C superconductor [3–6], yet the pressure needed for its formation is too high (~ 500 GPa) [7]. Ashcroft proposed to stabilize states similar to metallic hydrogen at lower pressures by creating hydrogen-rich hydrides, where the hydrogen atoms experience an additional “chemical” pressure [8]. Following this, many theoretical predictions of remarkable superconductors (HTSC) were made, e.g., in Ca-H [9], Y-H [10], H-S [11], Th-H [12], Ac-H [13], and La-H [10] systems. In all these systems, the high- T_C superconductors have unusual chemical compositions, e.g., H₃S, LaH₁₀, CaH₆. The formation of such compounds, violating the rules of classical chemistry, commonly takes place under pressure [15].

The first experimental proof was obtained for H₃S with measured $T_C = 203$ K at 155 GPa [16] (the predicted value was 191-204 K at 200 GPa [11]). The confidence in such predictions has greatly increased because of their agreement with the observations, and stimulated a wave of

theoretical studies of superconductivity in hydrides [10,12,13,16–29]. The recent theoretical work on La-H and Y-H systems [10] under pressure showed that LaH₁₀ and YH₁₀ at 300 GPa may display the room-temperature superconductivity (at 286-326 K). According to that theoretical study, at pressures below 200 GPa LaH₁₀ has the $R\bar{3}m$ symmetry, changing to $Fm\bar{3}m$ at higher pressures. In the experiments by Geballe et al. [20], $R\bar{3}m$ -LaH₁₀ was found at ≤ 160 -170 GPa, while $Fm\bar{3}m$ -LaH₁₀ was found at higher pressures. The experimentally observed sharp drop in resistivity in LaH₁₀ samples was the first evidence of superconductivity in this system [1,2]. Different studies showed a series of superconducting-like transitions with T_C of 70 and 112 K [1], 210-215 K [1], 244-250 K [1,2] and 260-280 K [1]. This discrepancy in T_C values may be caused by the coexistence of lanthanum hydrides having different compositions and crystal structures in the studied samples. To address these questions, we predicted the stable compounds in the La-H system using the variable-composition evolutionary algorithm USPEX [30–32]. While most calculations report only T_C (computed under assumption of μ^* being in the range 0.1-0.15), here we obtain T_C using different approaches including superconducting DFT (which requires no assumption of μ^*), and also compute other properties, such as critical magnetic field, which can be computed with experiment [1].

Computational details

The evolutionary algorithm USPEX [30–32] is a powerful tool for predicting thermodynamically stable compounds of given elements. To predict thermodynamically stable phases in the La-H system, we performed variable-composition crystal structure searches at pressures from 50 to 200 GPa. The first generation of 100 structures was created using a random symmetric [32] and topological structure generators [33] with the number of atoms in the primitive unit cell ranging from 8 to 16, while the subsequent generations contained 20% of random structures, and the rest 80% of structures were created using the heredity, softmutation and transmutation operators. Here, the evolutionary searches were combined with structure relaxations using the density functional theory (DFT) [34, 35] within the generalized gradient approximation (the Perdew-Burke-Ernzerhof functional) [36], and the projector-augmented wave method [37, 38] as implemented in the VASP package [39–41]. The plane wave kinetic energy cutoff was set to 500 eV and the Brillouin zone was sampled by Γ -centered k -points meshes with resolution $2\pi \times 0.05 \text{ \AA}^{-1}$. This methodology was used and proved to be very effective in our previous works (e.g., [12–14]).

The calculations of critical temperature and electron-phonon coupling (EPC) parameters were carried out using Quantum ESPRESSO (QE) package [42] within the density-functional perturbation theory [43], employing the plane-wave pseudopotential method and Perdew-Burke-Ernzerhof exchange-correlation functional [36]. Convergence tests showed that 90 Ry is a suitable kinetic energy cutoff for the plane wave basis set. Electronic band structures along with phonon densities of states were calculated using both VASP (finite displacement method using PHONOPY [44, 45]) and QE (density-functional perturbation theory [43]), which demonstrated good consistency.

In our calculations of the EPC parameter λ , the first Brillouin zone was sampled using a $4 \times 4 \times 4$ q -points mesh and a denser $16 \times 16 \times 16$ k -points mesh (with the Gaussian smearing and $\sigma = 0.02$ Ry, which approximates the zero-width limits in the calculation of λ).

The critical temperature was calculated from the Eliashberg equation [46] which is based on the Fröhlich Hamiltonian $\hat{H} = \hat{H}_e + \hat{H}_{ph} + \sum_{k,q,j} g_{k+q,k}^{q,j} \hat{c}_{k+q}^+ \hat{c}_k (\hat{b}_{-q,j}^+ + \hat{b}_{q,j})$, where c^+ , b^+ are creation operators of electrons and phonons, respectively. The matrix elements of the electron-phonon interaction $g_{k+q,k}^{q,j}$ were calculated within the harmonic approximation in Quantum ESPRESSO as follows:

$$\Delta_{nk}(T) = -Z_{nk}(T)\Delta_{nk}(T) - \frac{1}{2}\sum K_{nkn'k'}(T) \frac{\tanh\beta\xi_{n'k'}}{\xi_{n'k'}}\Delta_{n'k'}(T), \quad (1)$$

where u_q is the displacement of an atom with mass M in the phonon mode q,j . Within the approach of Gor'kov and Migdal [47, 48], the correction to the electron Green's function $\Sigma(\vec{k}, \omega) = G_0^{-1}(\vec{k}, \omega) - G^{-1}(\vec{k}, \omega)$ caused by the interaction can be calculated by taking into account only the first terms of the expansion of electron-phonon interaction in a series of (ω_{\log}/E_F) . This leads to the integral Eliashberg equations [46] which can be solved by the iterative self-consistent method for the real part of the order parameter $\Delta(T, \omega)$ (superconducting gap) and the mass renormalization function $Z(T, \omega)$ [49] (see Supporting Information).

For LaH₁₀ and LaH₁₆, we also estimated T_c and μ^* by solving the gap equation within the density functional theory for superconductors [50, 51] (SCDFT):

$$\Delta_{nk}(T) = -Z_{nk}(T)\Delta_{nk}(T) - \frac{1}{2}\sum K_{nkn'k'}(T) \frac{\tanh\beta\xi_{n'k'}}{\xi_{n'k'}}\Delta_{n'k'}(T), \quad (2)$$

The ‘‘order parameter’’ $\Delta_{nk}(T)$ does not depend on the frequency ω , but depends on the eigenstates of \hat{H}_e labeled by the band index n and wave vector k ; it is defined in a way different from that in the Eliashberg equation and is proportional to the thermal average $\langle c_{nk\uparrow}c_{n-k\downarrow} \rangle$, with $c_{nk\sigma}$ being the annihilation operator of the spin state $nk\sigma$ [50]. ξ_{nk} denotes the normal-state energy eigenvalue measured from the Fermi level. The interaction effects treated in the Eliashberg equation are included with the kernels entering this gap equation; $Z_{nk} = Z_{nk}^{ph}$; $K_{nkn'k'} = K_{nkn'k'}^{ph} + K_{nkn'k'}^{el}$. Here we included the mass-renormalization by the phonon exchange with $Z_{nk}^{ph} = Z^{ph}(\xi_{nk})$ (see Eq. (40) in [52] and an improved form of Eq. (24) in [51] to consider non-constant electronic density of states), the phonon-mediated electron-electron attraction with $K_{nkn'k'}^{PH} = K^{PH}(\xi_{nk}, \xi_{n'k'})$ (Eq. (23) in [51]), and the screened Coulomb repulsion $K_{nkn'k'}^{el}$ (Eq. (3) in [53]). Unlike the Eliashberg equation, the SCDFT gap equation does not contain the frequency ω . Nevertheless, the retardation effect [54] is approximately incorporated [51]. The absence of ω enables us to treat all electronic states in a wide energy range of ± 30 eV at an affordable computational cost, and therefore estimate T_c without the empirical Coulomb pseudopotential μ^* . We used this gap equation to estimate T_c as the temperature where its nontrivial solution vanishes (see Supporting Information for details).

The Sommerfeld constant was calculated using the following formula:

$$\gamma = \frac{2}{3}\pi^2 k_B^2 N(0)(1 + \lambda), \quad (3)$$

where λ is the EPC parameter, $N(0)$ – the electronic density of states at the Fermi level, k_B – the Boltzmann constant.

Results and Discussion

I. Stability of La-H phases

We performed the variable-composition evolutionary searches for stable compounds and crystal structures at 50, 100, 150 and 200 GPa. The thermodynamic convex hulls are shown in Fig. 1. By construction, stable phases are those that appear on the convex hull. Thus, at 50 GPa we found $Fm\bar{3}m$ -LaH, $Pnma$ -LaH₃, $Cmc2_1$ -LaH₇ and Cc -LaH₉ to be stable (Fig. 1a). At 100 GPa, LaH₇ and LaH₉ disappear from the convex hull, while four new hydrides become stable: Cm -LaH₂, $Cmcm$ -LaH₃, $P\bar{1}$ -LaH₅ and $P4/nmm$ -LaH₁₁ (Fig. 1b). At 150 GPa, the chemistry of lanthanum hydrides becomes much richer: $P6/mmm$ -LaH₂, $Cmcm$ -LaH₃, $I4/mmm$ -LaH₄, $P\bar{1}$ -LaH₅, $Fm\bar{3}m$ -LaH₁₀ and $P6/mmm$ -LaH₁₆ phases become stable (Fig. 1c). At 200 GPa, only five stable lanthanum hydrides remain on the convex hull: $P6/mmm$ -LaH₂, $Cmmm$ -La₃H₁₀, $I4/mmm$ -LaH₄, $Fm\bar{3}m$ -LaH₁₀, and $P6/mmm$ -LaH₁₆. Our results are similar to those from [55], the main difference being that we predict the new compounds LaH, La₃H₁₀

and LaH_{16} hydrides and also find that LaH_{10} is stable at pressures higher than 135 GPa (which is consistent with the experimental data from [1,2]). Yet, we found $Fm\bar{3}m$ - LaH_{10} to be more stable than $R\bar{3}m$ - LaH_{10} at pressure above 150 GPa. The $R\bar{3}m \rightarrow Fm\bar{3}m$ phase transition occurs at 128 GPa (Fig. S19 in Supporting Information). Taking into account the zero-point energy correction, the pressure of this phase transition shifts to 135 GPa, which is consistent with the experimental phase transition pressure of 160 GPa [20]. Below we will discuss the superconducting properties of the previously known lanthanum hydrides and explore the crystal structure and SC properties of the newly found LaH_{16} . The crystal structure data is summarized in Table S1 in Supporting Information.

Stoichiometry 1:1 is common for various hydrides (e.g., U-H [14], Fe-H [23], and many others [56]). $Fm\bar{3}m$ -LaH has a rocksalt-type structure, with La-H distance of 2.26 Å at 50 GPa. In the $Pnma$ - LaH_3 structure, La atoms have a 10-fold coordination and H-H distances, which are too long to be considered bonding (2.28 Å at 50 GPa). In $Cmc2_1$ - LaH_7 , the lanthanum atoms have a 13-fold coordination, while the shortest H-H distances (0.81 Å at 50 GPa) are clearly bonding and quite close to the H-H bond length in the molecular hydrogen (0.74 Å).

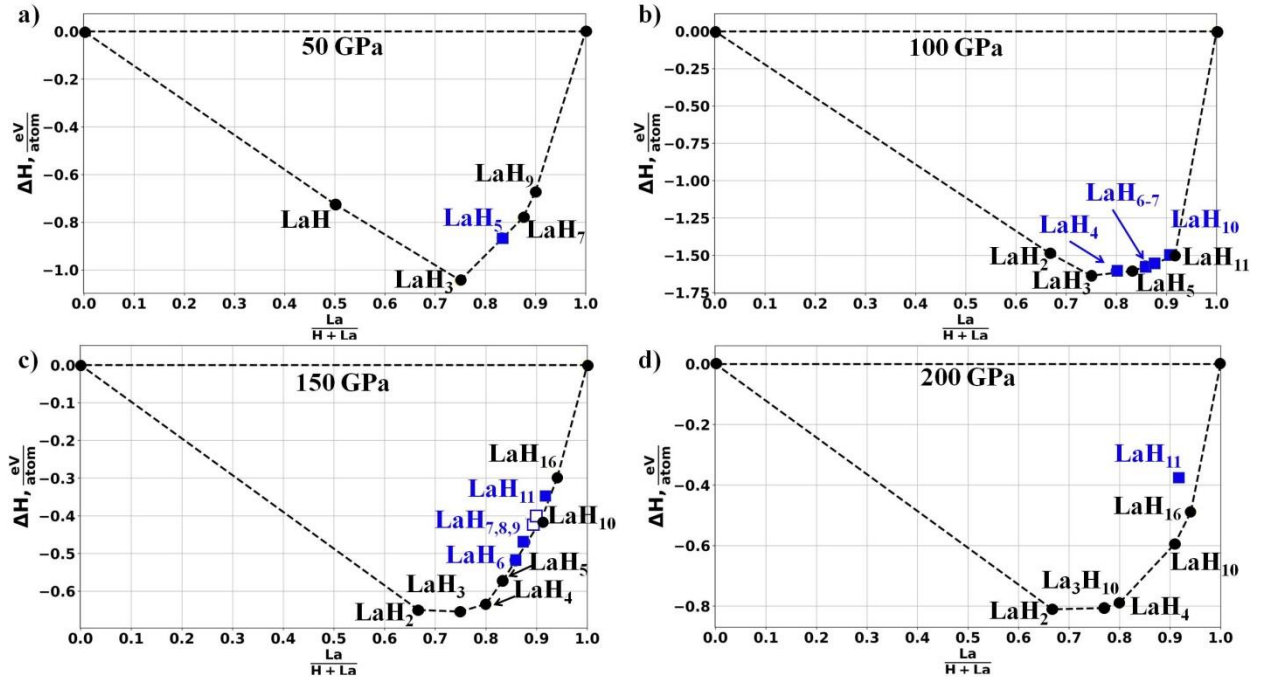


Fig. 1. Convex hull diagrams for the La-H system at a) 50, b) 100, c) 150, and d) 200 GPa. The metastable and stable phases are marked by blue squares and black circles, respectively.

Our results at 150 GPa are consistent with those in Ref. [10]: $P6/mmm$ - LaH_2 , $Cmcm$ - LaH_3 , $Immm$ - LaH_4 and $P\bar{1}$ - LaH_5 phases are thermodynamically stable. Previous studies explored only simple fixed stoichiometries, whereas USPEX method used here can automatically detect even nontrivial stoichiometries, which helped us find a new phase, $Cmmm$ - La_3H_{10} , at 200 GPa. This phase is structurally related to $Cmcm$ - LaH_3 , while its lattice parameter c is 3 times larger, and an additional hydrogen atom in the tripled unit cell.

II. Superconductivity of LaH_{10} phases

Superconductivity of LaH_{10} has been confirmed in experiments [1,2]. Our analysis is based on calculations of the Eliashberg function $\alpha^2F(\omega)$ and electronic density of states for $R\bar{3}m$ - and $Fm\bar{3}m$ - LaH_{10} phases. Experimental observations found the maximum T_C of ~ 251 K at 168 GPa [2] or $T_C \sim 260$ K at 180 GPa [1], i.e. close to the $R\bar{3}m - Fm\bar{3}m$ phase transition (but in the cubic phase). The value of Coulomb pseudopotential μ^* for LaH_{10} phases determined from SCDFE equals to 0.2 at 200 GPa (see Supporting Information).

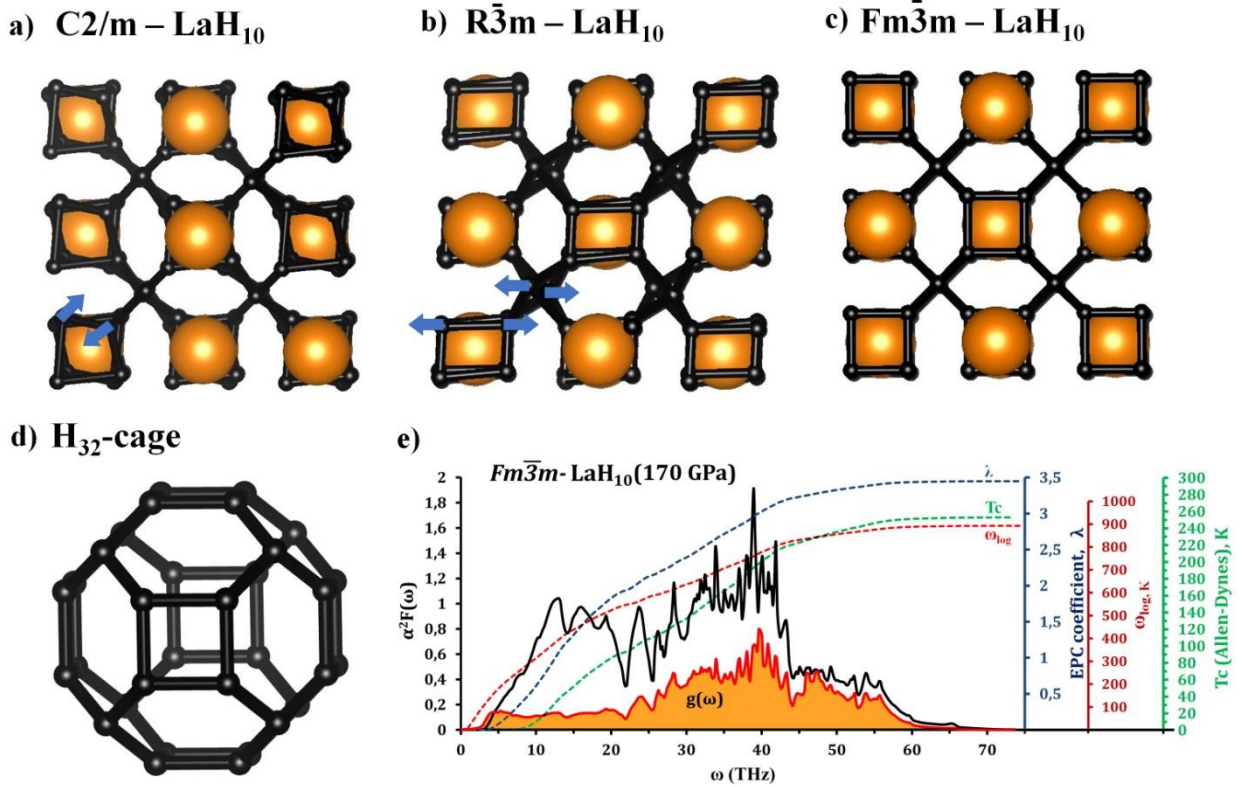


Fig. 2. Crystal structures of a) $C2/m$ - LaH_{10} , b) $R\bar{3}m$ - LaH_{10} , c) $Fm\bar{3}m$ - LaH_{10} ; d) hydrogen H_{32} cage common for these phases; e) Eliashberg $\alpha^2F(\omega)$ function (black curve), phonon density of states (orange) and cumulative ω_{\log} (red), EPC coefficient λ (blue), critical transition temperature T_C (green) of $Fm\bar{3}m$ - LaH_{10} at 170 GPa. Crystal structures were generated using VESTA software [57]; La and hydrogen atoms are shown as large orange and small black balls, respectively; blue arrows show displacements of hydrogen atoms in comparison with cubic H_8 cluster.

For $Fm\bar{3}m$ - LaH_{10} SCDFD gives a very high EPC coefficient $\lambda = 3.75$ and $T_C = 271$ K at 200 GPa (see Table 1 and Supporting Information for details). At 200 and 250 GPa, the calculated volumes (30.4 and 28.5 \AA^3 , respectively) and the electronic density of states $N(E_F) = N(0) = 10.6$ and 10.0 states/f.u./Ry allowed us to estimate the Sommerfeld constant (Table 1): 0.016 and 0.011 $\text{J/mol}\cdot\text{K}^2$ at 200 and 250 GPa, i.e. very close to that of $Fm\bar{3}m$ - ThH_{10} (0.011 $\text{J/mol}\cdot\text{K}^2$ [12]) at 100 GPa. These constants were used to calculate critical magnetic field ($\mu_0H_C(0)$) and jump in specific heat ($\Delta C/T_C$), see Table 1. For calculation details please see Supporting Information.

The Eliashberg function for cubic $Fm\bar{3}m$ - LaH_{10} at 200 GPa is shown in Fig. 2e (see Supporting Information for other pressure values and phases). At an experimental pressure of 170 GPa, the T_C of cubic LaH_{10} , calculated by the numerical solution of Eliashberg equation, is 259 K (Table 1), which is in good agreement with the theoretical results [10] and experiments [1,2].

The calculated critical temperature for $R\bar{3}m$ - LaH_{10} is 203 K at 150 GPa (Table 1), which is much lower than for $Fm\bar{3}m$ modification. Thus, $R\bar{3}m$ - LaH_{10} can explain the experimental results by Drozdov et al. [1].

Table 1. Parameters of the superconducting state of $Fm\bar{3}m$ -LaH₁₀ and $R\bar{3}m$ -LaH₁₀ from the Eliashberg equation (with $\mu^* = 0.2$).

Parameters	$Fm\bar{3}m$ -LaH ₁₀				$R\bar{3}m$ -LaH ₁₀	
	170 GPa	200 GPa	210 GPa	250 GPa	150 GPa	165 GPa
N_f , states/f.u./Ry	11.2	10.6	10.3	10.0	12.2	11.0
λ	3.94	3.75	3.42	2.29	2.77	2.63
ω_{\log} , K	801	906	851	1253	833	840
T_C , K	259	271*	249	246	203	197
$\Delta(0)$, meV	62.0	63.7	59.6	48.0	48.5	43.7
$\mu_0 H_C(0)$, T **	89.0	95.0	81.0	66.7	72.7	71.0
$\Delta C/T_C$, mJ/mol·K ²	31.5	44.7	34.5	33.4	42.8	25.7
γ , J/mol·K ²	0.019	0.016	0.015	0.011	0.018	0.018
$R_\Delta = 2\Delta(0)/k_B T_C$	5.54	5.46	5.55	5.00	5.55	5.54

*SCDFT, see Supporting Information.

** Experimentally measured critical magnetic field is 95-136 T [1]

The isotopic coefficient β calculated by the A-D formula (see Supporting Information) is 0.48 (using $\mu^* = 0.2$ for A-D equation) for $Fm\bar{3}m$ -LaH₁₀ at 200 GPa, the value for $R\bar{3}m$ -LaH₁₀ is the same. Using the isotopic coefficient β , we can determine the critical temperature of lanthanum deca-deuteride ($Fm\bar{3}m$ -LaD₁₀) as $T_D = 2^{-\beta} \cdot T_H = 181$ K, and 154 K for $R\bar{3}m$ -LaD₁₀. Experimentally measured T_C for $Fm\bar{3}m$ -LaD₁₀ is 168 K [1], which agrees with our prediction.

III. Prediction of high- T_C LaH₁₆

Perhaps the most intriguing finding of our work is that besides the hydrogen-rich LaH₁₀ phases we also predicted $P6/mmm$ -LaH₁₆ to be thermodynamically stable at pressures above 150 GPa (Fig. 1c). This phase has a different crystal structure from the previously predicted AcH₁₆ [13]. The lanthanum atoms form an *hcp* sublattice and are coordinated by 12 hydrogen atoms (Fig. 3a). These H-units consist of three parallel layers of hydrogen atoms. The distances between the hydrogen atoms in the first, second and third layers at 150 GPa are 1.07, 1.02 and 1.07 Å, respectively. The distance between the closest hydrogen atoms from different layers is 1.25 Å, so these layers form 2D infinite networks. The crystal structures of all predicted phases are summarized in Table S1 (see Supporting Information).

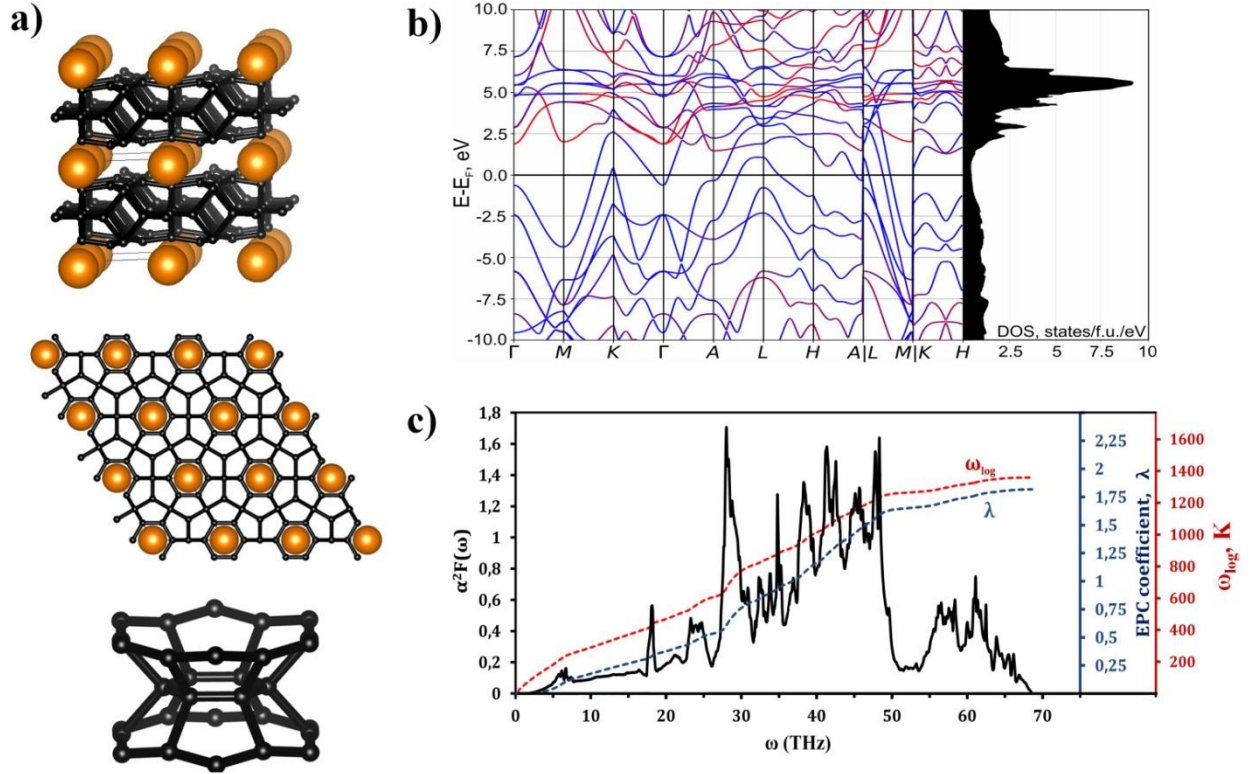


Fig. 3. a) Crystal structure of $P 6/mmm$ -LaH₁₆ at 150 GPa; b) band structure and DOS of LaH₁₆ (La — red, H — blue) at 250 GPa; c) Eliashberg function $\alpha^2F(\omega)$ (black), cumulative ω_{log} (red), and EPC coefficient λ (blue) of $P6/mmm$ -LaH₁₆ at 200 GPa.

$P 6/mmm$ -LaH₁₆ shows very little dependence of the electronic density of states on the pressure at 200-300 GPa. The computed Eliashberg function of $P 6/mmm$ -LaH₁₆ at 200 GPa is shown in Fig. 3c (see Supporting Information for other pressure values). The EPC coefficient of LaH₁₆ (Table 2) is approximately two times lower than that of LaH₁₀. SCDFPT calculations show that T_C of LaH₁₆ is 156 K at 200 GPa. This T_C value leads to the anomalously large $\mu^* = 0.41$ for LaH₁₆ compared to the commonly accepted interval (0.1-0.15). This abnormal value of μ^* (LaH₁₆) is caused by the complex behavior of DOS(E) in the vicinity of $E_F \pm 1$ eV (see Supporting Information). Thus, we used $\mu^* = 0.41$ in the numerical solution of the Eliashberg equation and calculated the superconducting properties of $P 6/mmm$ -LaH₁₆ (Table 2). T_C of this phase shows weak pressure dependence ($dT_C/dP = -0.3$ K/GPa).

Table 2. Parameters of the superconducting state of $P 6/mmm$ -LaH₁₆ at 200-300 GPa calculated using the Eliashberg equation at $\mu^* = 0.41$. Here γ is the Sommerfeld constant (calculated using eq. (3)).

Parameter	200 GPa	250 GPa	300 GPa
$N_f, \text{states/f.u./Ry}$	7.21	6.94	7.07
λ	1.82	1.63	1.44
ω_{log}, K	1362	1511	1675
T_C, K	156	141	118
$\Delta(0), \text{meV}$	29.6	25.7	20.2
$\mu_0 H_c(0), T$	35.0	29.9	23.6
$\Delta C/T_C, \text{mJ/mol}\cdot K^2$	18.6	15.1	12.4
$\gamma, \text{mJ/mol}\cdot K^2$	7.3	6.5	6.1
$R_A = 2\Delta(0)/k_B T_C$	4.5	4.2	4.0

IV. Superconductivity of lanthanum hydrides LaH_m ($m = 4-9, 11$)

As it was shown before, different lanthanum hydrides can undergo a series of superconducting transitions at different pressures with different T_C [1], so we checked other lanthanum hydrides. In this work we found a number of LaH_m phases ($m = 4 \dots 9, 11$) at different pressures, and it was very computationally expensive to calculate their T_C using the SCDF method. In this case we calculated T_C of LaH_m phases ($m = 4 \dots 9, 11$) using the Allen-Dynes (A-D) formula [58, 59] in the pressure range of 150-180 GPa, which is the experimentally studied pressure region [2], using the commonly accepted μ^* values (0.1-0.15). The calculated T_C values are shown in Fig. 4, and one can see that: (1) LaH_4 , LaH_6 and LaH_7 could explain the experimentally observed transition at ~ 215 K with the critical magnetic field $\mu_0 H_C(0) = 60-70$ T; (2) LaH_5 , LaH_8 , LaH_{11} could explain the experimentally observed transition at ~ 112 K with the critical magnetic field $\mu_0 H_C(0) = 20-25$ T. More details about the calculation of T_C in these phases can be found in Supporting Information.

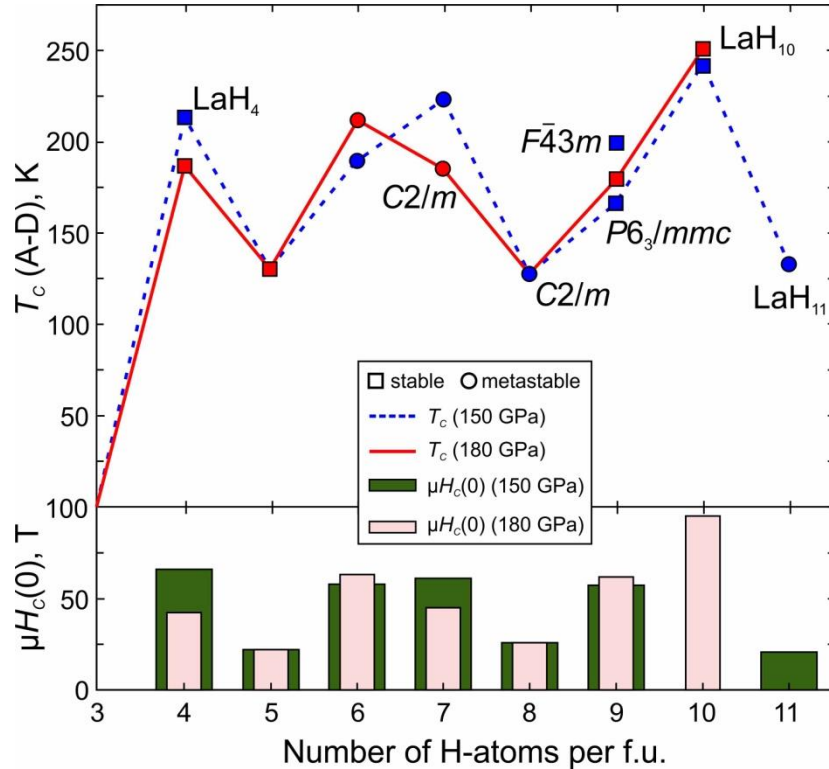


Fig. 4. Superconducting temperatures T_C (obtained with the A-D formula using $\mu^* = 0.1$) and critical magnetic fields for a series of lanthanum hydrides at 150 and 180 GPa.

Conclusions

Using the *ab initio* evolutionary algorithm USPEX, we predicted stable superconducting compounds in the La-H system at 50, 100, 150 and 200 GPa, including the previously unknown polyhydride $P6/mmm$ - LaH_{16} . The electronic, phonon, and superconducting properties of LaH_m with $m = 4-11$ were studied within the harmonic approximation, which gives possible explanations of the observed superconducting transitions at 70, 112, and 215 K [1]. The SCDF calculations for LaH_{10} and LaH_{16} led to unusually high values of μ^* (0.2-0.41), lying far outside the conventionally accepted interval, 0.1-0.15. The calculated Eliashberg function for $Fm\bar{3}m$ - LaH_{10} at 170 GPa gives $T_C = 259$ K, according to the numerical solution of the Eliashberg equation ($\mu^* = 0.2$). The critical magnetic field of $Fm\bar{3}m$ - LaH_{10} was found to be 89-95 T (73 T for the $R\bar{3}m$ phase), the harmonic isotope coefficient $\beta = 0.48$. The values of all the superconducting parameters for lanthanum hydrides are in good agreement with the available experimental data [1]. We found that $P6/mmm$ - LaH_{16} is a high-temperature superconductor with T_C of up to 156 K, the critical magnetic field of ~ 35 T and superconducting gap of 30 meV

at 200 GPa. The main conclusion of this comprehensive investigation is that even in one system the μ^* value may significantly vary and go beyond the commonly accepted interval, 0.1-0.15, which gives a special importance to the SCDFC calculations.

Acknowledgments

A.R.O. was supported by the Russian Science Foundation (grant 19-72-30043). A.G.K. thanks the RFBR foundation project № 19-03-00100 and FASIE for the financial support within the UMNK grant №13408GU/2018. The calculations were performed on the Rurik supercomputer at MIPT and the Arkuda supercomputer of the Skolkovo Foundation.

References

- [1] A. P. Drozdov, P. P. Kong, V. S. Minkov, S. P. Besedin, M. A. Kuzovnikov, S. Mozaffari, L. Balicas, F. F. Balakirev, D. E. Graf, V. B. Prakapenka, E. Greenberg, D. A. Knyazev, M. Tkacz, and M. I. Eremets, *Nature* **569**, 528 (2019).
- [2] M. Somayazulu, M. Ahart, A. K. Mishra, Z. M. Geballe, M. Baldini, Y. Meng, V. V. Struzhkin, and R. J. Hemley, *Phys. Rev. Lett.* **122**, 027001 (2019).
- [3] N. W. Ashcroft, *Phys. Rev. Lett.* **21**, 1748 (1968).
- [4] P. Cudazzo, G. Profeta, A. Sanna, A. Floris, A. Continenza, S. Massidda, and E. K. U. Gross, *Phys. Rev. Lett.* **100**, 257001 (2008).
- [5] P. Cudazzo, G. Profeta, A. Sanna, A. Floris, A. Continenza, S. Massidda, and E. K. U. Gross, *Phys. Rev. B* **81**, 134505 (2010).
- [6] P. Cudazzo, G. Profeta, A. Sanna, A. Floris, A. Continenza, S. Massidda, and E. K. U. Gross, *Phys. Rev. B* **81**, 134506 (2010).
- [7] R. P. Dias and I. F. Silvera, *Science* eaal1579 (2017).
- [8] N. W. Ashcroft, *Phys. Rev. Lett.* **92**, 187002 (2004).
- [9] H. Wang, J. S. Tse, K. Tanaka, T. Iitaka, and Y. Ma, *Proc. Natl. Acad. Sci.* **109**, 6463 (2012).
- [10] H. Liu, I. I. Naumov, R. Hoffmann, N. W. Ashcroft, and R. J. Hemley, *Proc. Natl. Acad. Sci.* **114**, 6990 (2017).
- [11] D. Duan, Y. Liu, F. Tian, D. Li, X. Huang, Z. Zhao, H. Yu, B. Liu, W. Tian, and T. Cui, *Sci. Rep.* **4**, 6968 (2014).
- [12] A. G. Kvashnin, D. V. Semenok, I. A. Kruglov, and A. R. Oganov, *ACS Appl. Mater. Interfaces* **10**, 43809 (2018).
- [13] D. V. Semenok, A. G. Kvashnin, I. A. Kruglov, and A. R. Oganov, *J. Phys. Chem. Lett.* **9**, 1920 (2018).
- [14] W. Zhang, A. R. Oganov, A. F. Goncharov, Q. Zhu, S. E. Boulfelfel, A. O. Lyakhov, M. Somayazulu, and V. B. Prakapenka, *Science* **342**, 1502 (2013).
- [15] A. P. Drozdov, M. I. Eremets, I. A. Troyan, V. Ksenofontov, and S. I. Shylin, *Nature* **525**, 73 (2015).
- [16] I. A. Kruglov, A. G. Kvashnin, A. F. Goncharov, A. R. Oganov, S. S. Lobanov, N. Holtgrewe, Sh. Jiang, V. B. Prakapenka, E. Greenberg, and A. V. Yanilkin, *Sci Adv* **4**, eaat9776 (2018).
- [17] D. Duan, Y. Liu, Y. Ma, Z. Shao, B. Liu, and T. Cui, *Natl. Sci. Rev.* **4**, 121 (2017).
- [18] A. K. Mishra, M. Somayazulu, M. Ahart, A. Karandikar, R. J. Hemley, and V. V. Struzhkin, in *Bull. Am. Phys. Soc.* (2018).
- [19] P. P. Kong, A. P. Drozdov, E. Eroko, and M. I. Eremets, in *Book Abstr. AIRAPT 26 Jt. ACHPR 8 CHPC 19* (Beijing, China, 2017), p. 347.
- [20] Z. M. Geballe, H. Liu, A. K. Mishra, M. Ahart, M. Somayazulu, Y. Meng, M. Baldini, and R. J. Hemley, *Angew. Chem. Int. Ed.* **57**, 688 (2017).
- [21] C. M. Pépin, G. Geneste, A. Dewaele, M. Mezouar, and P. Loubeyre, *Science* **357**, 382 (2017).

- [22] A. Majumdar, J. S. Tse, M. Wu, and Y. Yao, *Phys. Rev. B* **96**, 201107 (2017).
- [23] A. G. Kvashnin, I. A. Kruglov, D. V. Semenok, and A. R. Oganov, *J. Phys. Chem. C* **122**, 4731 (2018).
- [24] N. P. Salke, M. M. D. Esfahani, Y. Zhang, I. A. Kruglov, J. Zhou, Y. Wang, E. Greenberg, V. B. Prakapenka, A. R. Oganov, and J.-F. Lin, ArXiv:1805.02060 <https://arxiv.org/ftp/arxiv/papers/1805/1805.02060.pdf> (2018).
- [25] H. Wang, J. S. Tse, K. Tanaka, T. Iitaka, and Y. Ma, *Proc. Natl. Acad. Sci.* **109**, 6463 (2012).
- [26] K. Tanaka, J. S. Tse, and H. Liu, *Phys. Rev. B* **96**, 100502 (2017).
- [27] G. Gao, R. Hoffmann, N. W. Ashcroft, H. Liu, A. Bergara, and Y. Ma, *Phys. Rev. B* **88**, 184104 (2013).
- [28] K. Abe, *Phys. Rev. B* **96**, 144108 (2017).
- [29] X. Li and F. Peng, *Inorg. Chem.* **56**, 13759 (2017).
- [30] A. R. Oganov and C. W. Glass, *J Chem Phys* **124**, 244704 (2006).
- [31] A. R. Oganov, A. O. Lyakhov, and M. Valle, *Acc. Chem. Res.* **44**, 227 (2011).
- [32] A. O. Lyakhov, A. R. Oganov, H. T. Stokes, and Q. Zhu, *Comput. Phys. Commun.* **184**, 1172 (2013).
- [33] P. V. Bushlanov, V. A. Blatov, and A. R. Oganov, *Comput. Phys. Commun.* **236**, 1 (2019).
- [34] P. Hohenberg and W. Kohn, *Phys Rev* **136**, B864 (1964).
- [35] W. Kohn and L. J. Sham, *Phys Rev* **140**, A1133 (1965).
- [36] J. P. Perdew, K. Burke, and M. Ernzerhof, *Phys. Rev. Lett.* **77**, 3865 (1996).
- [37] P. E. Blöchl, *Phys. Rev. B* **50**, 17953 (1994).
- [38] G. Kresse and D. Joubert, *Phys. Rev. B* **59**, 1758 (1999).
- [39] G. Kresse and J. Furthmüller, *Phys. Rev. B* **54**, 11169 (1996).
- [40] G. Kresse and J. Hafner, *Phys. Rev. B* **47**, 558 (1993).
- [41] G. Kresse and J. Hafner, *Phys. Rev. B* **49**, 14251 (1994).
- [42] P. Giannozzi, S. Baroni, N. Bonini, M. Calandra, R. Car, C. Cavazzoni, D. Ceresoli, G. L. Chiarotti, M. Cococcioni, I. Dabo, A. D. Corso, S. de Gironcoli, S. Fabris, G. Fratesi, R. Gebauer, U. Gerstmann, C. Gougoussis, A. Kokalj, M. Lazzeri, L. Martin-Samos, N. Marzari, F. Mauri, R. Mazzarello, S. Paolini, A. Pasquarello, L. Paulatto, C. Sbraccia, S. Scandolo, G. Sclauzero, A. P. Seitsonen, A. Smogunov, P. Umari, and R. M. Wentzcovitch, *J. Phys. Condens. Matter* **21**, 395502 (2009).
- [43] S. Baroni, S. de Gironcoli, A. Dal Corso, and P. Giannozzi, *Rev. Mod. Phys.* **73**, 515 (2001).
- [44] A. Togo and I. Tanaka, *Scr. Mater.* **108**, 1 (2015).
- [45] A. Togo, F. Oba, and I. Tanaka, *Phys. Rev. B* **78**, 134106 (2008).
- [46] G. M. Eliashberg, *JETP* **11**, 696 (1959).
- [47] L. P. Gor'kov, *JETP* **34**, 735 (1958).
- [48] A. B. Migdal, *JETP* **34**, 996 (1958).
- [49] E. G. Maksimov, D. Y. Savrasov, and S. Y. Savrasov, *Phys.-Uspekhi* **40**, 337 (1997).
- [50] M. Lüders, M. A. L. Marques, N. N. Lathiotakis, A. Floris, G. Profeta, L. Fast, A. Continenza, S. Massidda, and E. K. U. Gross, *Phys. Rev. B* **72**, 024545 (2005).
- [51] M. A. L. Marques, M. Lüders, N. N. Lathiotakis, G. Profeta, A. Floris, L. Fast, A. Continenza, E. K. U. Gross, and S. Massidda, *Phys. Rev. B* **72**, 024546 (2005).
- [52] R. Akashi and R. Arita, *Phys. Rev. B* **88**, 014514 (2013).
- [53] R. Akashi, M. Kawamura, S. Tsuneyuki, Y. Nomura, and R. Arita, *Phys. Rev. B* **91**, 224513 (2015).
- [54] P. Morel and P. W. Anderson, *Phys. Rev.* **125**, 1263 (1962).
- [55] F. Peng, Y. Sun, C. J. Pickard, R. J. Needs, Q. Wu, and Y. Ma, *Phys. Rev. Lett.* **119**, 107001 (2017).
- [56] D. V. Semenok, I. A. Kruglov, A. G. Kvashnin, and A. R. Oganov, ArXiv180600865 *Cond-Mat* (2018).

- [57] K. Momma and F. Izumi, *J. Appl. Crystallogr.* **44**, 1272 (2011).
- [58] P. B. Allen and R. C. Dynes, *Phys. Rev. B* **12**, 905 (1975).
- [59] J. P. Carbotte, *Rev. Mod. Phys.* **62**, 1027 (1990).

Supporting Information

Superconductivity in LaH₁₀ and LaH₁₆ polyhydrides

Ivan A. Kruglov,^{1,2,} Dmitrii V. Semenov,^{1,3} Hao Song⁹, Radosław Szczęśniak,^{4,5} Izabela A. Wrona,⁴ Ryosuke Akashi,⁶ M. Mahdi Davari Esfahani,⁷ Defang Duan,⁹ Tian Cui,⁹ Alexander G. Kvashnin^{3,1} and Artem R. Oganov^{3,2,8}*

¹ Moscow Institute of Physics and Technology, 141700, 9 Institutsky lane, Dolgoprudny, Russia

² Dukhov Research Institute of Automatics (VNIIA), Moscow 127055, Russia

³ Skolkovo Institute of Science and Technology, Skolkovo Innovation Center 143026, 3 Nobel Street, Moscow, Russia

⁴ Institute of Physics, Jan Dlugosz University in Czestochowa, Ave. Armii Krajowej 13/15, 42-200 Czestochowa, Poland

⁵ Institute of Physics, Czestochowa University of Technology, Ave. Armii Krajowej 19, 42-200 Czestochowa, Poland

⁶ University of Tokyo, 7-3-1 Hongo, Bunkyo, Tokyo 113-8654, Japan

⁷ Department of Geosciences and Center for Materials by Design, Institute for Advanced Computational Science, State University of New York, Stony Brook, NY 11794-2100, USA

⁸ International Center for Materials Discovery, Northwestern Polytechnical University, Xi'an, 710072, China

⁹ Key State Laboratory of Superhard Materials, Jilin University, Changchun, China

Corresponding Author

*Ivan A. Kruglov, E-mail: ivan.kruglov@phystech.edu

*Dmitrii V. Semenov, E-mail: Dmitrii.Semenov@skoltech.ru

*Artem R. Oganov, E-mail: A.Oganov@skoltech.ru

Content

Crystal data of La-H phases	2
Equations for calculating T_C and related parameters	3
Calculation of critical magnetic field for LaH₁₀ phases	9
Superconductivity of lanthanum hydrides LaH_m ($m = 4-9, 11$)	10
Electronic and phonon properties of La-H phases	12
Eliashberg spectral functions	17
Stability of LaH₁₀ polymorphs	20
Matlab functions for T_C calculation using Allen's algorithm from Ref. 10	21
References	23

Crystal data of La-H phases

Table S1. Crystal structures of predicted La-H phases.

Phase	Pressure, GPa	Lattice parameters	Coordinates			
			La			
$Fm\bar{3}m$ -LaH	50	a = 4.53 Å	La	0.5	0.5	0.5
			H	0.0	0.0	0.0
$Pnma$ -LaH ₃	50	a = 7.20 Å, b = 4.57 Å, c = 3.67 Å	La	-0.365	0.25	-0.320
			H	0.394	-0.001	-0.171
			H	0.356	0.25	0.332
$Cmc2_1$ -LaH ₇	50	a = 7.20 Å, b = 4.57 Å, c = 3.67 Å	La	0.0	-0.159	-0.452
			H	0.0	0.466	0.408
			H	0.0	0.245	-0.300
			H	0.0	-0.365	0.241
			H	0.0	0.174	0.420
			H	0.25	0.417	0.237
$P6/mmm$ -LaH ₂	150	a = 2.80 Å, c = 2.72 Å	La	0.0	0.0	0.0
			H	0.333	0.667	0.5
$Cmcm$ -LaH ₃	150	a = 2.76 Å, b = 10.69 Å, c = 2.80 Å	La	0.0	0.118	0.25
			H	0.0	0.467	0.25
			H	0.0	0.313	0.25
			H	0.0	-0.25	0.25
$Cmmm$ -La ₃ H ₁₀	150	a = 16.70 Å, b = 2.77 Å, c = 2.75 Å	La	-0.326	0.0	0.5
			La	0.0	0.0	0.0
			H	-0.089	0.0	0.5
			H	0.128	0.0	0.0
			H	-0.228	0.0	0.0
			H	-0.449	0.0	0.5
$I4/mmm$ -LaH ₄	150	a = 2.74 Å, c = 6.03 Å	La	0.0	0.0	0.5
			H	0.0	0.5	0.25
			H	0.0	0.0	-0.153
$P\bar{1}$ -LaH ₅	150	a = 2.91 Å, b = 5.26 Å, c = 3.47 Å, $\alpha = 93.34$, $\beta = 110.24$, $\gamma = 98.71$	La	-0.327	-0.266	-0.273
			H	0.263	0.036	-0.255
			H	0.073	0.431	-0.280
			H	-0.067	0.122	-0.349
			H	-0.304	0.375	-0.108
			H	-0.376	0.112	-0.151
$R\bar{3}m$ -LaH ₁₀	150	a = 3.66 Å, c = 8.53 Å	La	0.0	0.0	0.5
			H	0.0	0.0	0.097
			H	-0.168	0.168	0.276
			H	0.0	0.0	-0.259
$Fm\bar{3}m$ -LaH ₁₀	150	a = 5.08 Å	La	0.0	0.0	0.0
			H	-0.378	-0.378	-0.378
			H	0.25	0.25	0.25
$P6/mmm$ -LaH ₁₆	150	a = 3.68 Å, c = 3.70 Å	La	0.0	0.0	0.0
			H	-0.276	0.0	0.5
			H	0.5	0.0	0.245
			H	0.333	0.667	-0.203

Equations for calculating T_C and related parameters

The superconducting transition temperature was calculated by solving the gap equation derived from the density functional theory for superconductors (SCDFT) [1,2], where no empirical parameter such as μ^* was used. The nk -averaged formula for K^{ph} [Eq.(23) in Ref. [2]] and Z^{ph} [Eq.(40) in Ref. [3]] were employed to use the calculated $\alpha^2F(\omega)$. The nk -dependent

formula for K^{ph} [Eq.(3) in Ref. [4]] was used, which includes the dynamical as well as static screening effect on the Coulomb repulsion. The dielectric matrices $\epsilon(i\omega)$ were represented with the auxiliary plane-wave energy cutoff of 12.8 Ry and were calculated within the random-phase approximation [5] and electron-electron Coulomb matrix elements were evaluated as

$$W_{n\mathbf{k},n'\mathbf{k}'}(i\omega) = \langle \psi_{n\mathbf{k}} \psi_{n'\mathbf{k}'} | \epsilon^{-1}(i\omega) V | \psi_{n'\mathbf{k}'} \psi_{n\mathbf{k}} \rangle \quad (\text{S1})$$

where V is being the bare Coulomb interaction. Low-energy Kohn-Sham states were accurately treated with the weighted random sampling scheme in solving the gap equation, as described in Ref. [2]. The Kohn-Sham energy eigenvalues and matrix elements for the sampled states were evaluated by the linear interpolation from the data on equal meshes. The detailed conditions are summarized in Table S2.

Table S2. Summary of the detailed conditions for the Tc calculation with the SCDFT scheme.

Class	Parameter	LaH ₁₀ 200GPa	LaH ₁₆ 200GPa
charge density	k	16x16x16 equal mesh	16x16x16 equal mesh
	interpolation	1st order Hermite Gaussian [5] with width 0.050Ry	
dielectric matrix	k for bands crossing E_F	15x15x15 equal mesh	15x15x15 equal mesh
	k for other bands	5x5x5 equal mesh	5x5x5 equal mesh
	number of unoccupied bands ^a	57	75
	interpolation	Tetrahedron with the Rath-Freeman treatment [6]	
DOS for phononic kernels	k	21x21x21 equal mesh	21x21x21 equal mesh
	interpolation	Tetrahedron with the Blöchl correction [7]	
SCDFT gap function	number of unoccupied bands ^b	24	36
	k for the electronic kernel	5x5x5 equal mesh	5x5x5 equal mesh
	k for the KS energies	21x21x21 equal mesh	21x21x21 equal mesh
	Sampling points for bands crossing E_F	6000	6000
	Sampling points for the other bands	200	200
	Sampling error in Tc (%)	~2.6	~1.9
SC parameters	Critical temperature (T _C)	271	156
	Coloumb pseudopotential μ^* (E)	0.20	0.41
	μ^* (Allen-Dynes)	0.11	0.198

^a States up to $E_F+70\text{eV}$ are taken into account.

^b States up to $E_F+40\text{eV}$ are taken into account.

Isotopic coefficient β_{AD} was calculated using the Allen-Dynes interpolation formulas:

$$\beta_{McM} = -\frac{d \ln T_C}{d \ln M} = \frac{1}{2} \left[1 - \frac{1.04(1+\lambda)(1+0.62\lambda)}{[\lambda - \mu^*(1+0.62\lambda)]^2} \mu^{*2} \right] \quad (\text{S2})$$

$$\beta_{\text{AD}} = \beta_{McM} - \frac{2.34\mu^{*2}\lambda^{3/2}}{(2.46+9.25\mu^*) \cdot ((2.46+9.25\mu^*)^{3/2} + \lambda^{3/2})} - \frac{130.4 \cdot \mu^{*2}\lambda^2(1+6.3\mu^*) \left(1 - \frac{\omega_{\text{log}}}{\omega_2}\right) \frac{\omega_{\text{log}}}{\omega_2}}{\left(8.28+104\mu^* + 329\mu^{*2} + 2.5 \cdot \lambda^2 \frac{\omega_{\text{log}}}{\omega_2}\right) \cdot \left(8.28+104\mu^* + 329\mu^{*2} + 2.5 \cdot \lambda^2 \left(\frac{\omega_{\text{log}}}{\omega_2}\right)^2\right)} \quad (\text{S3})$$

where the last two correction terms are usually small (~ 0.01).

The critical temperature of superconducting transition was calculated using Matsubara-type linearized Eliashberg equations: [8]

$$\hbar\omega_j = \pi(2j+1) \cdot k_B T, \quad j=0, \pm 1, \pm 2, \dots \quad (\text{S4})$$

$$\lambda(\omega_i - \omega_j) = 2 \int_0^\infty \frac{\omega \cdot \alpha^2 F(\omega)}{\omega^2 + (\omega_i - \omega_j)^2} d\omega \quad (\text{S5})$$

$$\Delta(\omega = \omega_i, T) = \Delta_i(T) = \pi k_B T \sum_j \frac{[\lambda(\omega_i - \omega_j) - \mu^*]}{\rho + \left| \hbar \omega_j + \pi k_B T \sum_k (\text{sign } \omega_k) \cdot \lambda(\omega_j - \omega_k) \right|} \cdot \Delta_j(T) \quad (S6)$$

where T is temperature in Kelvins, μ^* is Coloumb pseudopotential, ω is frequency in Hz, $\rho(T)$ is a pair-breaking parameter, function $\lambda(\omega_i - \omega_j)$ relates to effective electron-electron interaction *via* exchange of phonons. [9] Transition temperature can be found as a solution of equation $\rho(T_C) = 0$ where $\rho(T)$ is defined as $\max(\rho)$ providing that $\Delta(\omega)$ is not a zero function of ω at fixed temperature.

These equations can be rewritten in a matrix form as [10]

$$\rho(T) \psi_m = \sum_{n=0}^N K_{mn} \psi_n \Leftrightarrow \rho(T) \begin{pmatrix} \psi_1 \\ \dots \\ \psi_N \end{pmatrix} = \begin{pmatrix} K_{11} & \dots & K_{1N} \\ \dots & K_{ii} & \dots \\ K_{N1} & \dots & K_{NN} \end{pmatrix} \times \begin{pmatrix} \psi_1 \\ \dots \\ \psi_N \end{pmatrix}, \quad (S7)$$

where ψ_n relates to $\Delta(\omega, T)$, and

$$K_{mn} = F(m-n) + F(m+n+1) - 2\mu^* - \delta_{mn} \left[2m+1 + F(0) + 2 \sum_{l=1}^m F(l) \right] \quad (S8)$$

$$F(x) = F(x, T) = 2 \int_0^{\omega_{\max}} \frac{\alpha^2 F(\omega)}{(\hbar \omega)^2 + (2\pi \cdot kT \cdot x)^2} \cdot \hbar^2 \omega d\omega, \quad (S9)$$

where $\delta_{mn} = 1$ and $\delta_{nm} = 0$ ($n \neq m$) – is a unit matrix. Now one can replace criterion of $\rho(T_C) = 0$ by the vanishing of the maximum eigenvalue of the matrix K_{nm} : $\{\rho = \max_eigenvalue(K_{nm}) = f(T), f(T_C) = 0\}$.

We have implemented this simple approach, proposed by Philip Allen in 1974, as Matlab functions, shown at the last page of Supporting Information, which read files with $\alpha^2 F$ functions and carry out the calculations of T_C .

Exact calculations for $P6/mmm$ -LaH₁₆ at 250 GPa were also made using the Eliashberg equations in the following form (on the imaginary axis) [8]:

$$\phi_n = \frac{\pi}{\beta} \sum_{m=-M}^M \frac{\lambda(i\omega_n - i\omega_m) - \mu^* \theta(\omega_c - |\omega_m|)}{\sqrt{(\hbar \omega_m Z_m)^2 + \phi_m^2}} \phi_m \quad (S10)$$

$$Z_n = 1 + \frac{1}{\omega_n} \frac{\pi}{\beta} \sum_{m=-M}^M \frac{\lambda(i\omega_n - i\omega_m)}{\sqrt{(\hbar \omega_m Z_m)^2 + \phi_m^2}} \omega_m Z_m \quad (S11)$$

where: ϕ_n is the order parameter function, Z_n is the wave function renormalization factor, $\theta(x)$ is Heaviside function, $\hbar \omega_n = \pi \cdot k_B T \cdot (2n-1)$ is the n -th Matsubara frequency, $\beta = 1/k_B T$, μ^* is Coulomb pseudopotential, ω_c is the cut-off energy ($\omega_c = 3\Omega_{\max}$, Ω_{\max} is the maximum frequency in $\alpha^2 F(\omega)$). The electron-phonon pairing kernel is defined as:

$$\lambda(z) = 2 \int_0^{\Omega_{\max}} \frac{\alpha^2 F(\Omega)}{\Omega^2 - z^2} \Omega d\Omega. \quad (S12)$$

The Eliashberg equations were solved for 2201 Matsubara frequencies, starting from $T_0 = 10$ K (below this temperature, the solutions are not stable). The methods discussed in the papers [11–13] were used during the calculations.

The full form of the order parameter and the wave function renormalization factor on the real axis was obtained through analytical extension of the Eliashberg equations solutions from the imaginary axis, using the formula:

$$X(\omega) = \frac{p_1 + p_2\omega + \dots + p_r\omega^{r-1}}{q_1 + q_2\omega + \dots + q_r\omega^{r-1} + \omega^r}, \quad (\text{S13})$$

where $X \in \{\Delta; Z\}$, $r = 50$. The values of p_j and q_j parameters were selected in accordance with the principles presented in work [14]. Obtained results allow one to calculate dimensionless parameter R_C (relative jump of the specific heat), using the formula below:

$$R_C = \frac{C^S(T_C) - C^N(T_C)}{C^N(T_C)} \quad (\text{S14})$$

Because of strong-coupling and retardation effects in LaH_{10} and LaH_{16} , parameter R_C differs significantly from BCS theory prediction, in which the constant value is equal to 1.43. [15]

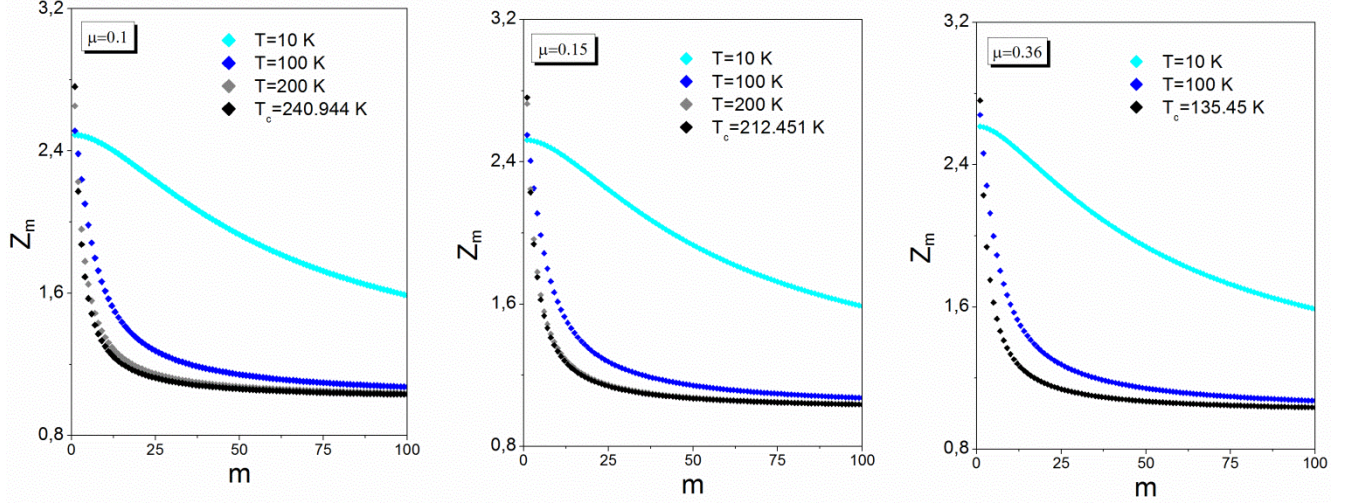


Fig. S1. The wave function renormalization factor for $P6/mmm\text{-LaH}_{16}$ at 250 GPa on the imaginary axis for the selected values of temperature (the first 100 values).

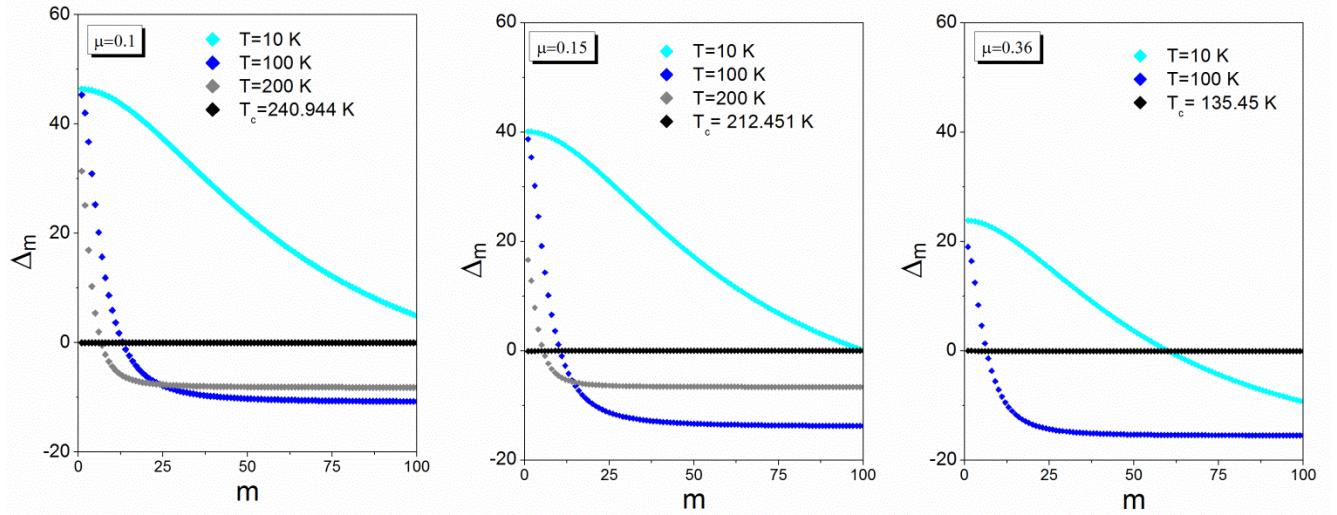


Fig. S2. The order parameter (in meV) for $P6/mmm\text{-LaH}_{16}$ at 250 GPa on the imaginary axis for the selected values of temperature (the first 100 values) and Coloumb pseudopotential.

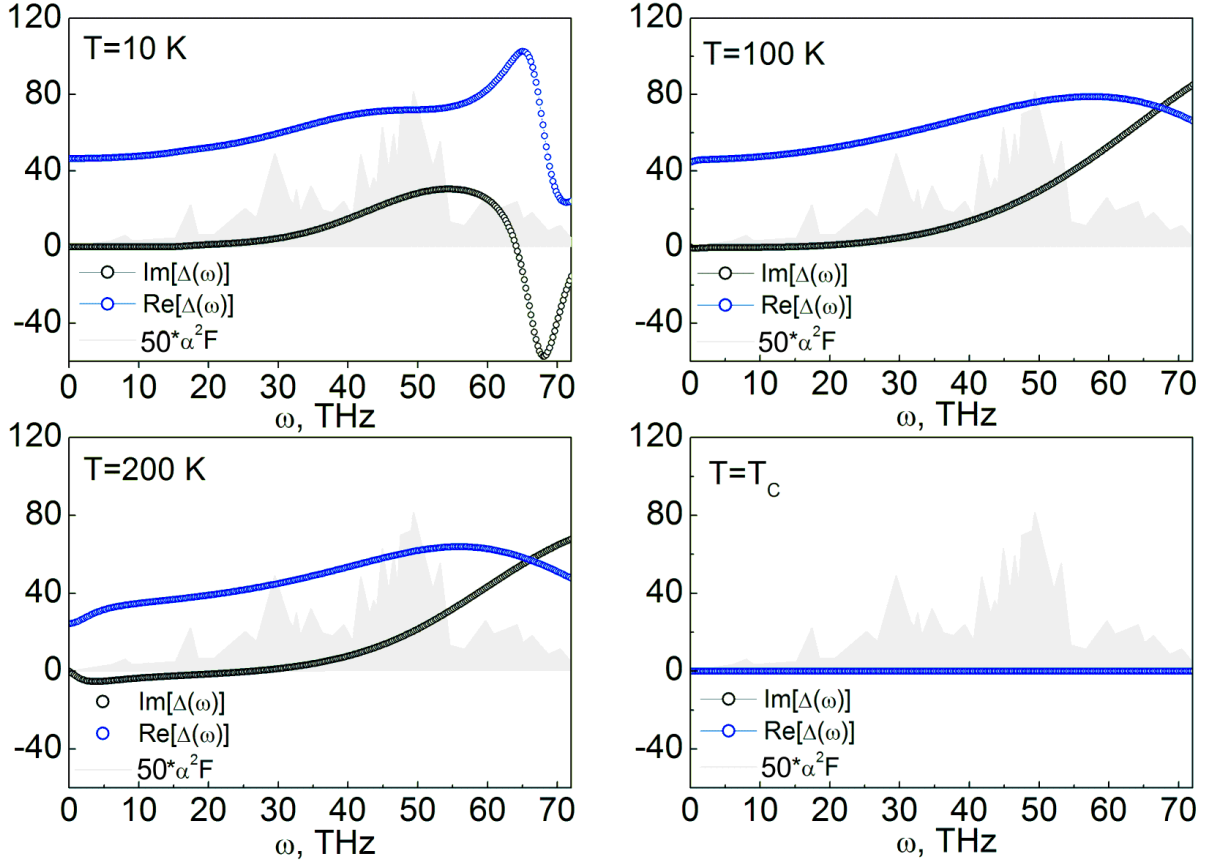


Fig. S3. The order parameter $\Delta(\omega)$ in meV for $P6/mmm$ -LaH₁₆ at 250 GPa on the real axis for the selected values of temperature ($\mu^* = 0.1$). In addition, the Eliashberg function (grey) was added as the background (multiplied by 50 for easier comparison).

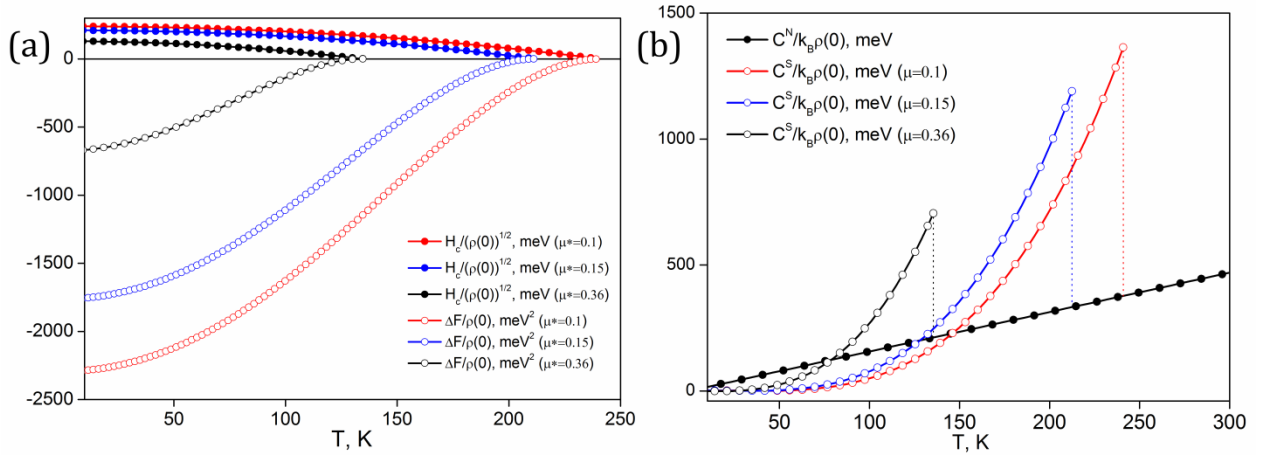


Fig. S4. a) The dependence of the thermodynamic critical field on the temperature (in meV, solid circles) and free energy difference between the superconducting state and the normal state as a function of the temperature (in meV², open circles); b) The specific heat of the superconducting state (C_S) and the normal state (C_N) as a function of temperature. Here $\rho(0)$ is the density of states at the Fermi level.

Table S3. Parameters of superconductive state of $P6/mmm$ -LaH₁₆ at 250 GPa calculated by the Eliashberg equations at different μ^*

Parameter	$P6/mmm$ -LaH ₁₆ (250 GPa)		
	$\mu^*=0.1$	$\mu^*=0.15$	$\mu^*=0.36$

T_C , K	241	213	135
$\Delta(0)$, meV	46.4	40.1	23.9
$\mu_0 H_C(0)$, T	52.3	45.8	28.4
$\Delta C/T_C$, mJ/mol·K ²	17.3	17.2	15.4
γ , mJ/mol·K ²	6.3	6.3	6.3
$R_A = 2\Delta(0)/k_B T_C$	4.47	4.38	4.09

Calculation of critical magnetic field for LaH₁₀ phases

Further study of superconductivity in $Fm\bar{3}m$ -LaH₁₀ implies investigation of the behavior of samples in the magnetic field. Using semi-empirical formulas of BCS theory (see Ref. [16], eq. 5.11 and 5.9):

$$\frac{\gamma T_C^2}{H_C^2(0)} = 0.168 \left[1 - 12.2 \left(\frac{T_C}{\omega_{\log}} \right)^2 \ln \left(\frac{\omega_{\log}}{3T_C} \right) \right] \quad (\text{S15})$$

and

$$\frac{\Delta C(T_C)}{\gamma T_C} = 1.43 \left[1 + 53 \left(\frac{T_C}{\omega_{\log}} \right)^2 \ln \left(\frac{\omega_{\log}}{3T_C} \right) \right], \quad (\text{S16})$$

we estimated the critical magnetic field and the jump in specific heat for $Fm\bar{3}m$ -LaH₁₀ in harmonic approximation (see Table 2). The superconducting gap was estimated by well-known semi-empirical equation, working satisfactorily for $T_C/\omega_{\log} < 0.25$ (see equation 4.1 in Ref. [16]):

$$\frac{2\Delta(0)}{k_B T_C} = 3.53 \left[1 + 12.5 \left(\frac{T_C}{\omega_{\log}} \right)^2 \ln \left(\frac{\omega_{\log}}{2T_C} \right) \right] \quad (\text{S17})$$

Estimation of the critical magnetic field for $Fm\bar{3}m$ -LaH₁₀ gives $\mu_0 H_C(0) \sim 89\text{-}95$ T at 170-200 GPa, which is greater than 70 T for H₃S [17] and agrees with lower bound of recent experimental results of 95-136 T [18].

Superconductivity of lanthanum hydrides LaH_m ($m = 4-9, 11$)

According to Ref. [18], pure LaH_3 is not a superconductor at all investigated pressures (0-200 GPa), but higher hydrides of La are metallic and superconducting. As it was shown earlier for LaH_{10} by SCDFT calculations, μ^* for A-D equation is 0.2, which is higher than the commonly accepted interval (0.1-0.15). Superconducting properties of all predicted hydrides were computed by Allen-Dynes (A-D) formula [19,16] at the pressure range 150-180 GPa, which is the experimentally studied pressure region [18].

Surprisingly, $I4/mmm\text{-LaH}_4$ demonstrates very strong electron-phonon coupling (see Table S4). At 150 GPa the $T_C(\text{A-D})$ is found to be 206 K and it decreases to 186 K at 180 GPa with $dT_C/dP \approx -0.67$ K/GPa. Thus, $I4/mmm\text{-LaH}_4$ could explain superconducting transition with $T_C = 215$ K observed in Ref. [18].

$P\bar{1}\text{-LaH}_5$ is stable at pressures above 150 GPa (Fig. 1c) and has T_C of 104-130 K at 150 GPa (see Table S4), almost insensitive to pressure ($dT_C/dP \approx -0.033$ K/GPa). This could explain the superconducting transition observed at $T_C \sim 112$ K [18].

$R\bar{3}m\text{-LaH}_6$ is metastable, but at 150 GPa it is very close to the convex hull (only 6 meV/atom above it, see Fig. 1c). Its electronic density of states is approximately pressure-independent, and its T_C increases with pressure ($dT_C/dP \approx +0.73$ K/GPa), because of the increase of the characteristic phonon frequency with pressure. According to our calculations, T_C of this phase can reach 211 K at 180 GPa (see Table S4).

Table S4. Predicted superconducting properties of slightly metastable and stable lanthanum hydrides. μ^* was taken as 0.1 (0.15).

Phase	P , GPa	λ	N_f states/f.u./Ry	ω_{\log} , K	T_C (A-D), K	$\mu_0 H_C(0)$, T
$I4/mmm\text{-LaH}_4$ ^{b)}	150	2.6	8.43	936	206 (179)	59 (52)
	180	1.6	7.62	1351	186 (157)	42(35)
$P\bar{1}\text{-LaH}_5$ ^{b)}	150	1.21	5.57 ^{a)}	1307	130 (104)	22 (17)
	180	1.15		1389	129 (102)	
$R\bar{3}m\text{-LaH}_6$	150	2.89	9.04 ^{a)}	765	189 (163)	58 (51)
	180	2.60		956	211 (183)	63 (55)
$C2/m\text{-LaH}_7$	150	2.94	7.21	894	223 (193)	61 (54)
	180	1.92	7.55	1102	185 (158)	45 (38)
$C2/m\text{-LaH}_8$ ^{c)}	150	1.56	6.32 ^{a)}	944	128 (107)	26 (21)
	180	1.53		950	127 (106)	
$P6_3/mmc\text{-LaH}_9$	150	2.75	11.6 ^{a)}	702	166 (144)	57 (50)
	180	2.98		708	180 (156)	62 (55)
$F\bar{4}3m\text{-LaH}_9$	150	2.92	7.72	802	199 (172)	56 (49)
$P4/nmm\text{-LaH}_{11}$	150	1.54	3.94	986	133 (111)	21 (17)

a) no changes with pressure; b) stable phase; c) from Ref. [20].

$C2/m\text{-LaH}_7$ is also metastable (17 meV/atom above the convex hull at 150 GPa, Fig. 1c) and displays T_C up to 223 K (with $dT_C/dP \approx -1.26$ K/GPa), see Table 3. This phase may be responsible for observed transition at ~ 215 K [18]. Metastable $C2/m\text{-LaH}_8$, proposed in Ref. [20], has $T_C = 106\text{-}127$ K (Table S4), which is almost insensitive to pressure.

For metastable LaH_9 we considered two polymorphs: isostructural to recently found $P6_3/mmc\text{-CeH}_9$ [21] and $F\bar{4}3m\text{-UH}_9$ [22]. We predict $T_C = 144\text{-}166$ K (150 GPa, Table S4) for hexagonal modification with $dT_C/dP = +0.46$ K/GPa. Obtained value is higher than that for CeH_9 [21,23]. For cubic LaH_9 T_C is higher: up to 199 K at 150 GPa (Table S4). Metastable $P4/nmm\text{-LaH}_{11}$ at 150-180 GPa shows relatively low $T_C = 111\text{-}133$ K (due to low density of states at Fermi level).

Electronic and phonon properties of La-H phases

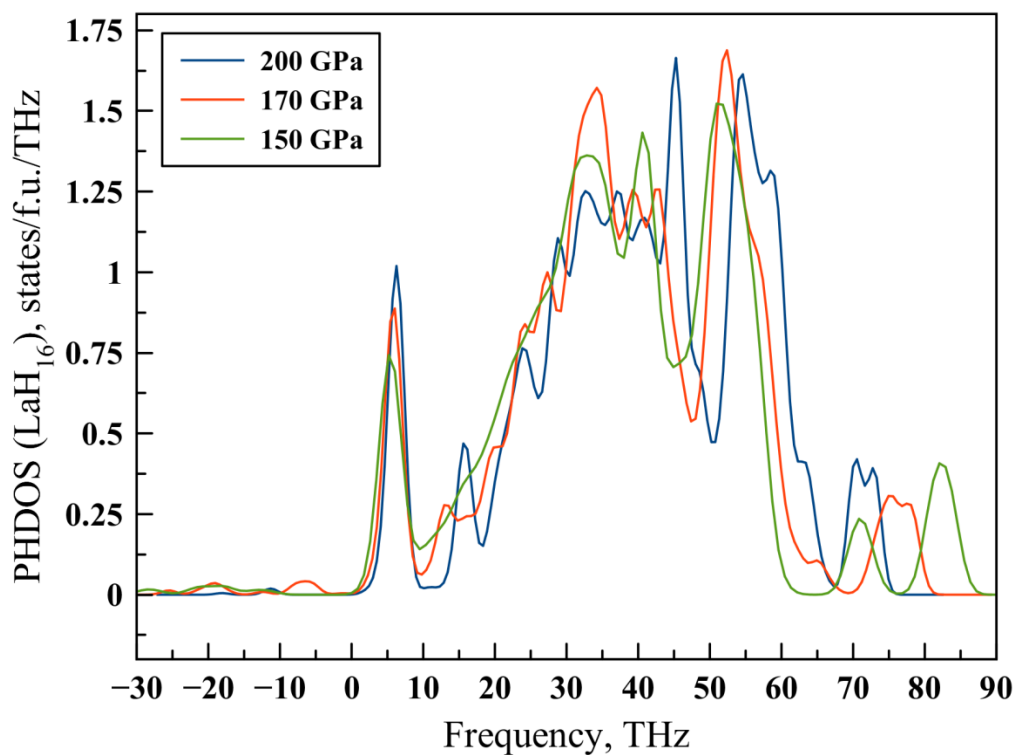


Fig. S5. Phonon density of states (DOS) of $P6/mmm$ - LaH_{16} phase at 150, 170 and 200 GPa.

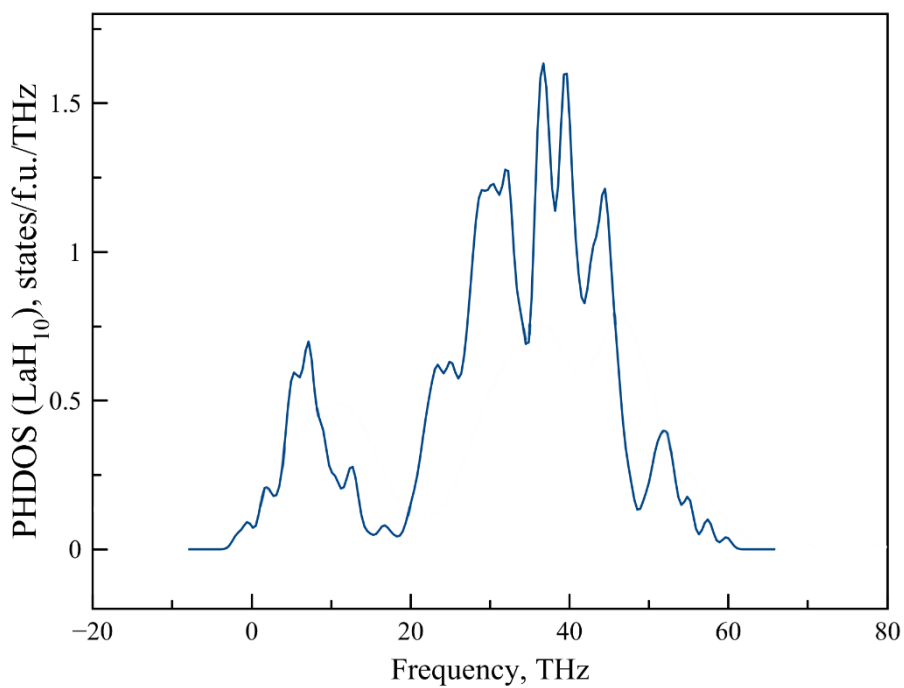


Fig. S6. Phonon density of states (smoothed) of $Fm\bar{3}m$ - LaH_{10} at 150 GPa.

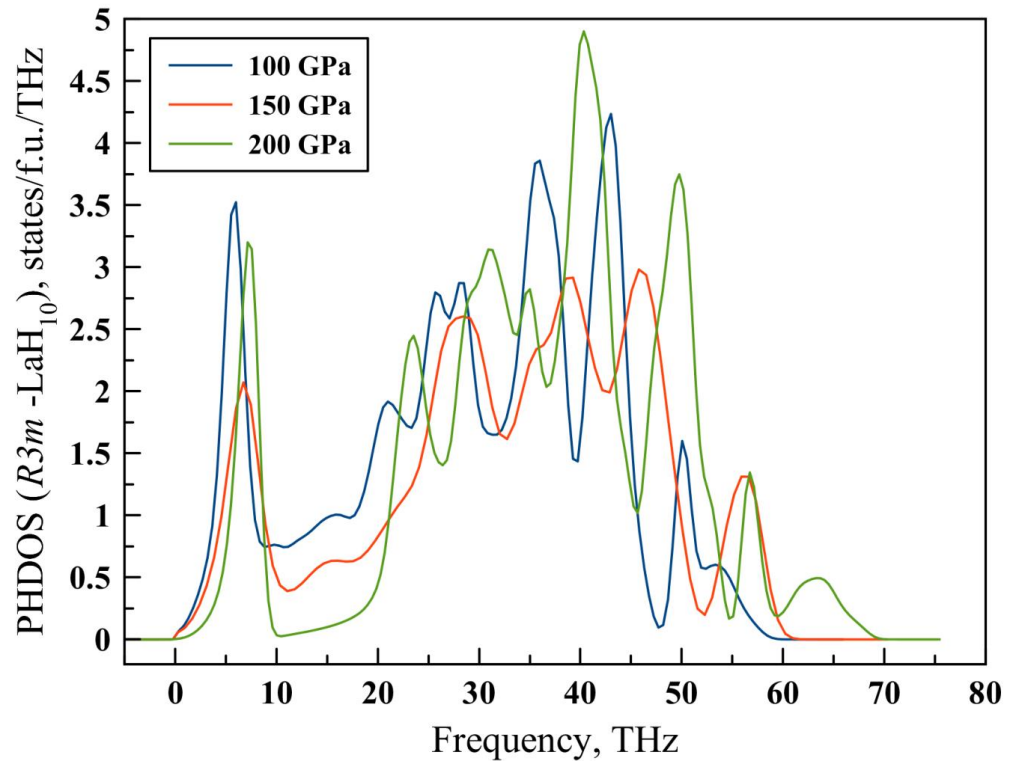


Fig. S7. Phonon density of states (smoothed) of $R\bar{3}m$ -LaH₁₀ at 100, 150 and 200 GPa.

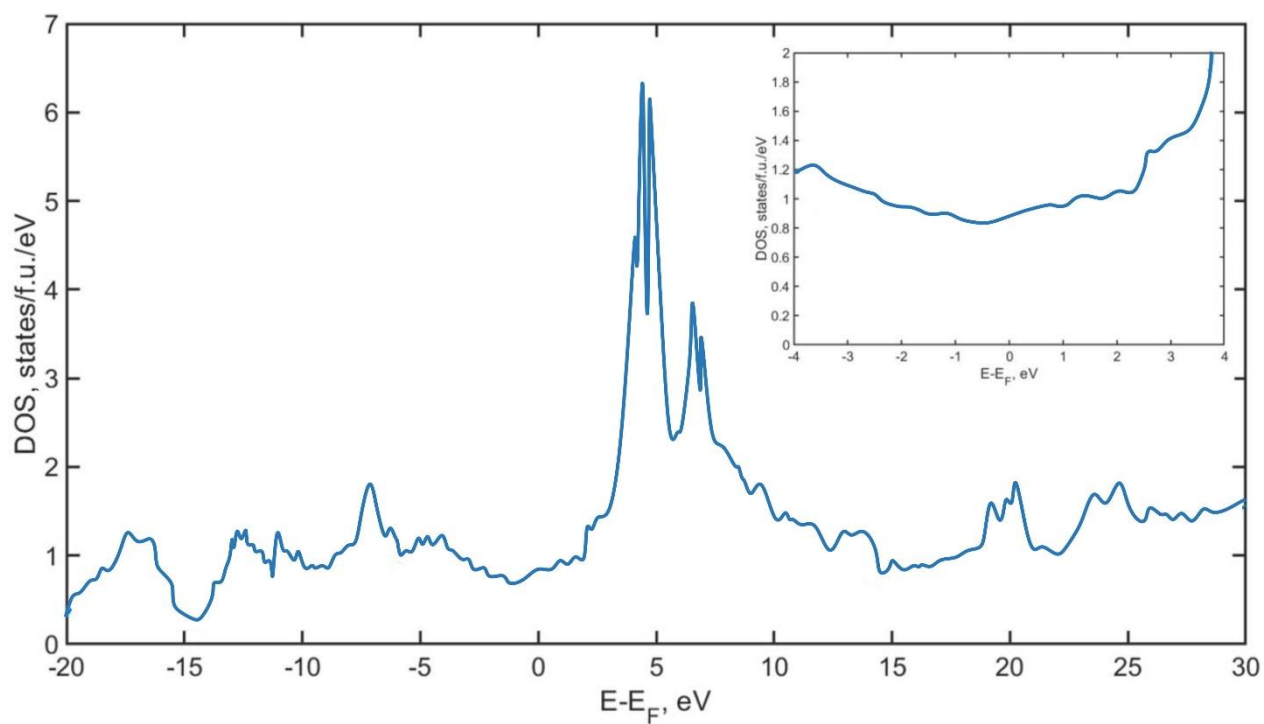


Fig. S8. Electronic density of states of $Fm\bar{3}m$ -LaH₁₀ at 200 GPa.

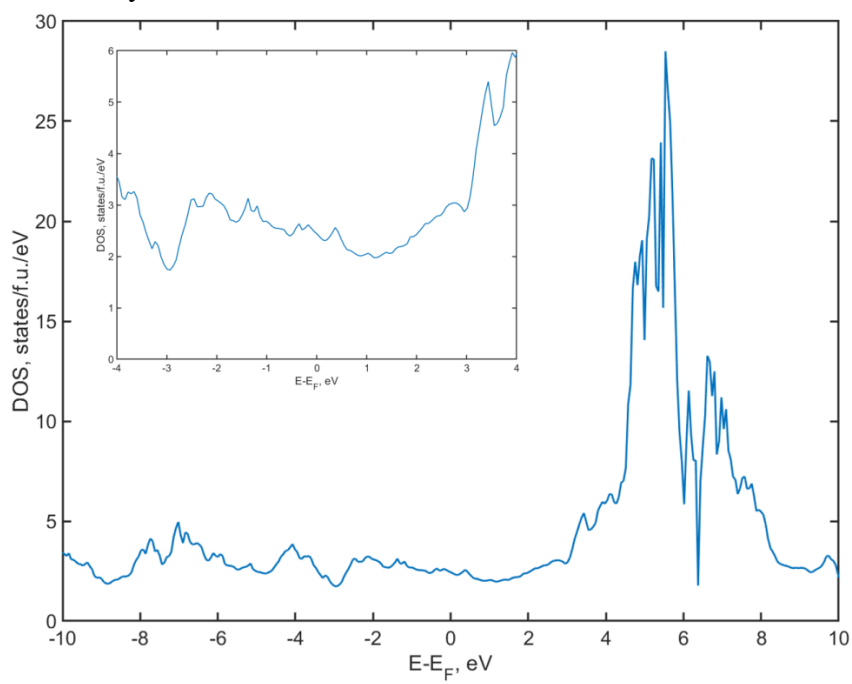


Fig. S9. Electronic density of states of $R\bar{3}m$ -LaH₁₀ at 165 GPa.

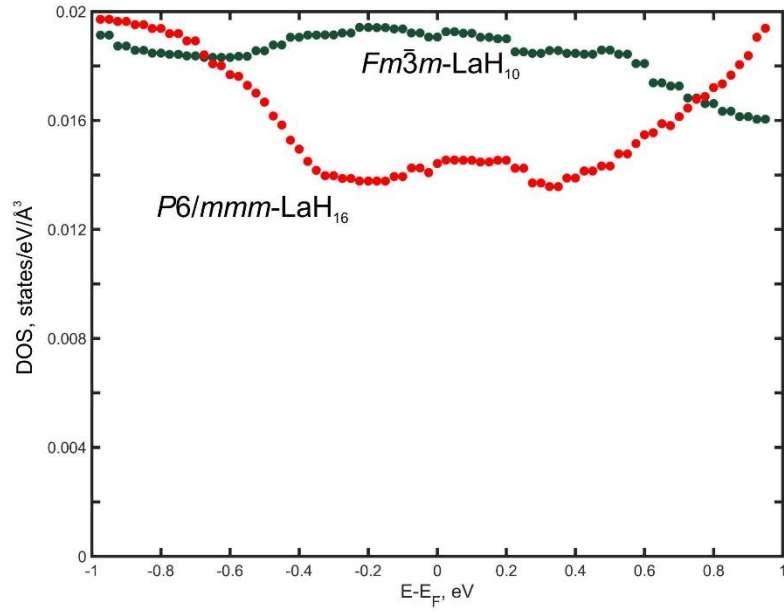


Fig. S10. Electronic density of states around the Fermi level in $Fm\bar{3}m$ -LaH₁₀ and $P6/mmm$ -LaH₁₆ at 200 GPa.

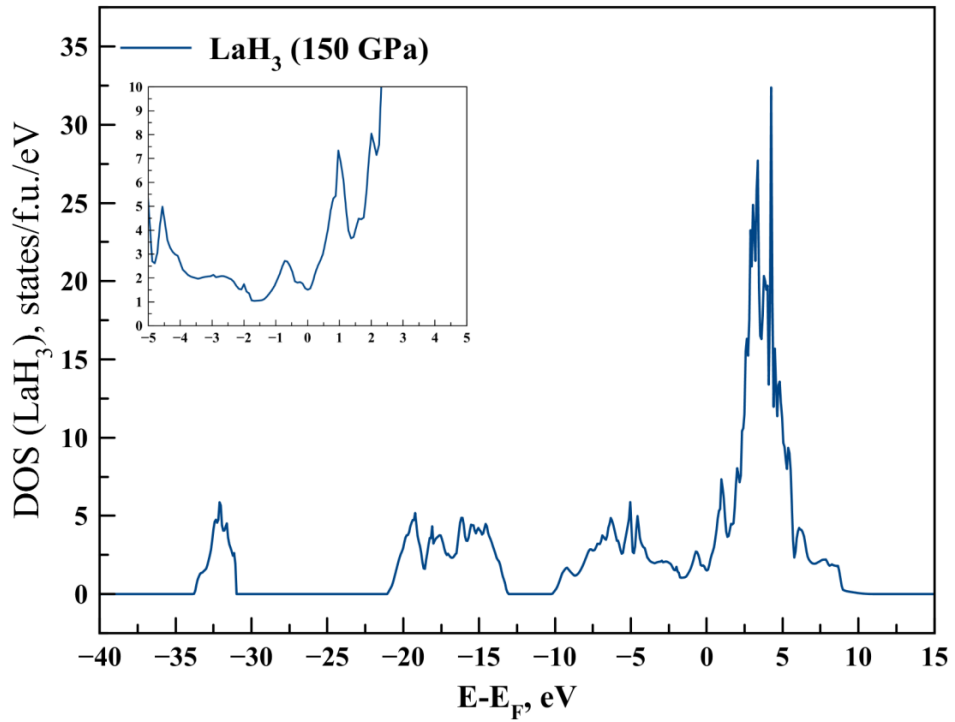


Fig. S11. Electronic density of states of $Cmcm$ -LaH₃ at 150 GPa.

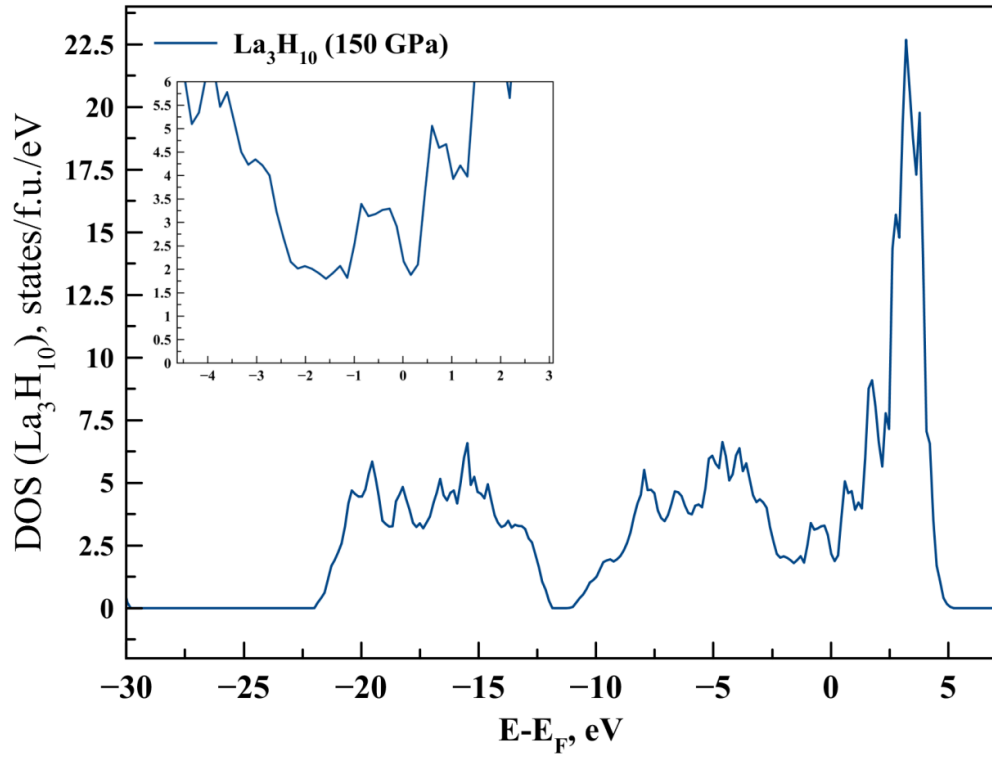


Fig. S12. Electronic density of states of $Cmmm$ - La_3H_{10} at 150 GPa.

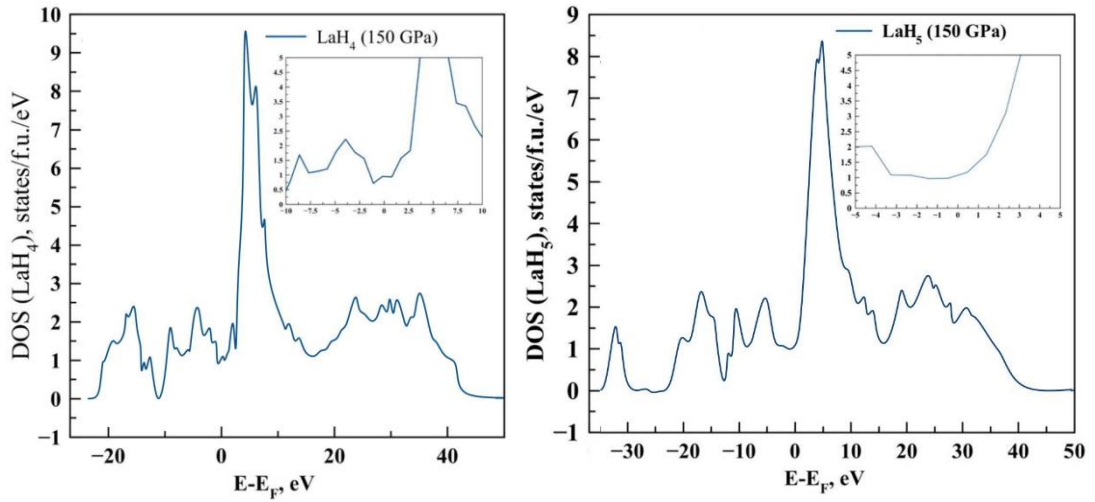


Fig. S13. Electronic density of states of $I4/mmm$ - LaH_4 and $P\bar{1}$ - LaH_5 at 150 GPa.

Eliashberg spectral functions

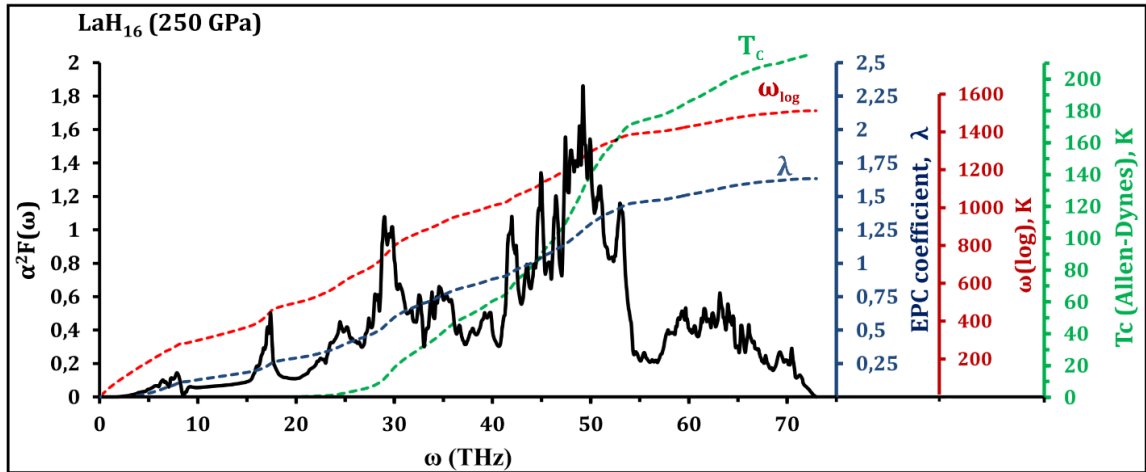


Fig. S14. Eliashberg function $\alpha^2F(\omega)$ (black), ω_{log} (red), EPC coefficient λ (blue), critical transition temperature T_c (green) of $P6/mmm$ -LaH₁₆ at 250 GPa.

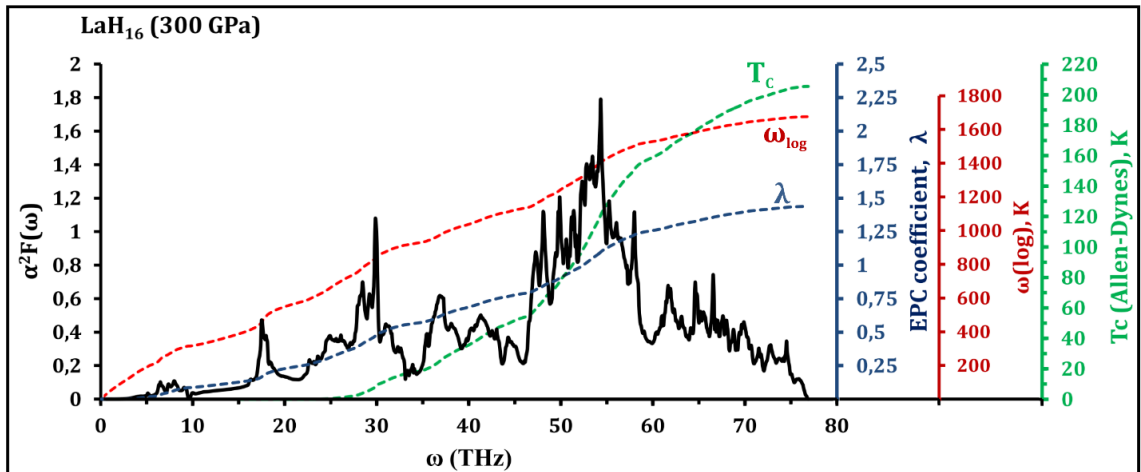


Fig. S15. Eliashberg function $\alpha^2F(\omega)$ (black), ω_{log} (red), EPC coefficient λ (blue), critical transition temperature T_c (green) of $P6/mmm$ -LaH₁₆ at 300 GPa.

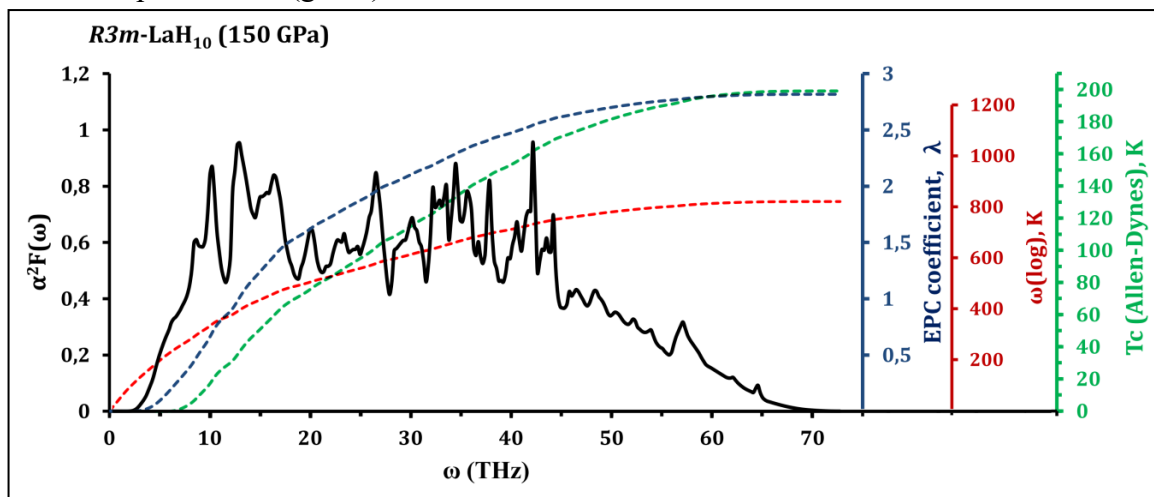


Fig. S16. Eliashberg function $\alpha^2F(\omega)$ (black), ω_{log} (red), EPC coefficient λ (blue), critical transition temperature T_c (green) of $R\bar{3}m$ -LaH₁₀ at 150 GPa.

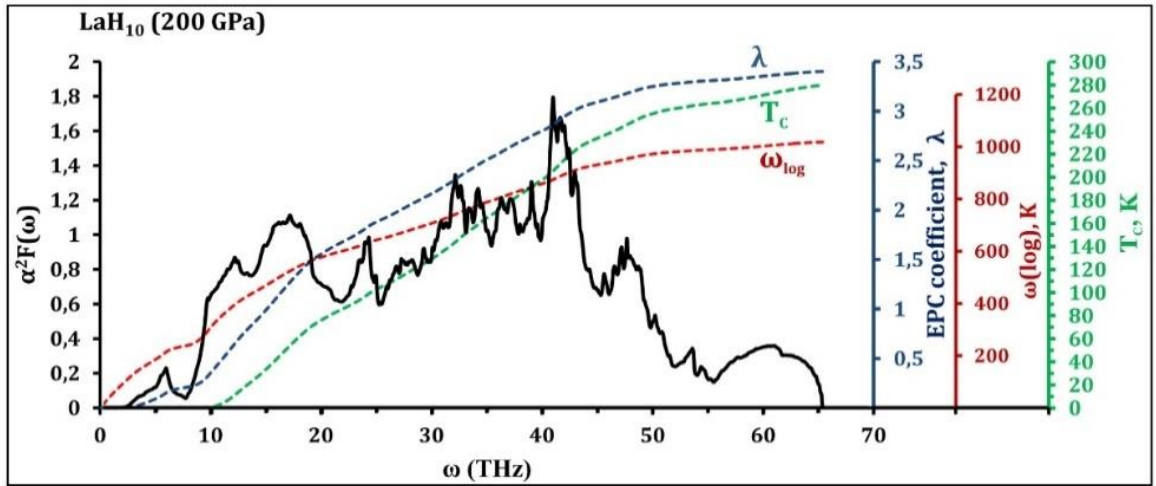


Fig. S17. Eliashberg $\alpha^2F(\omega)$ function (black curve), and cumulative ω_{\log} (red), EPC coefficient λ (blue), critical transition temperature T_c (green) of $Fm\bar{3}m$ -LaH₁₀ at 200 GPa.

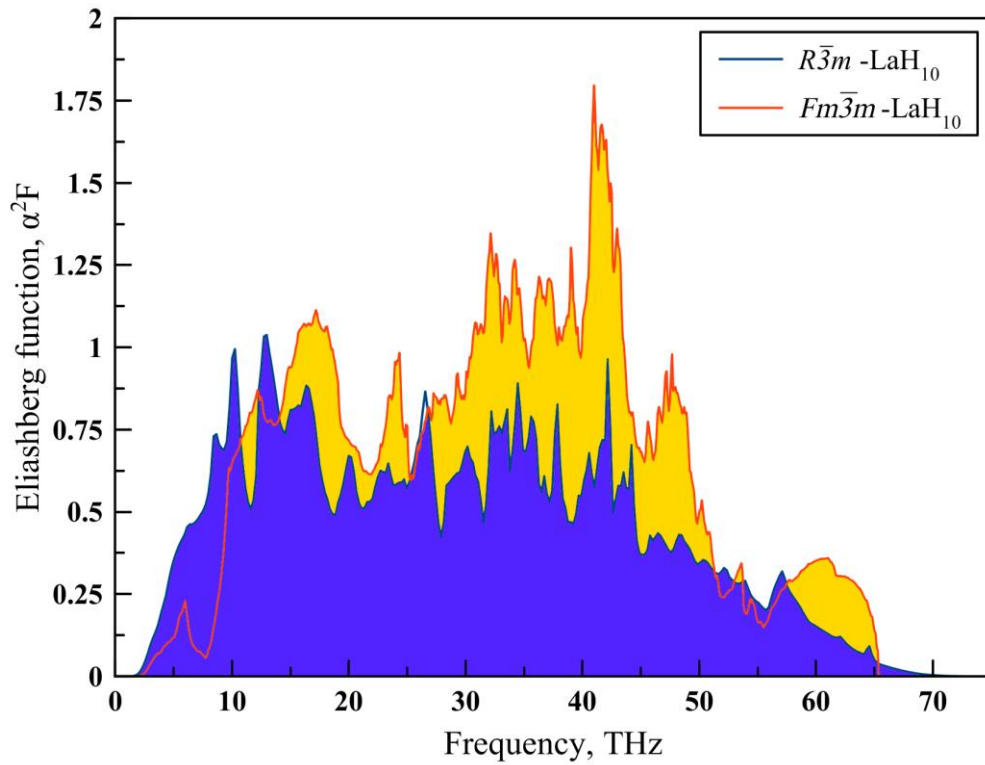


Fig. S18. Eliashberg functions $\alpha^2F(\omega)$ of $R\bar{3}m$ -LaH₁₀ at 150 GPa (blue) and $Fm\bar{3}m$ -LaH₁₀ at 200 GPa (yellow).

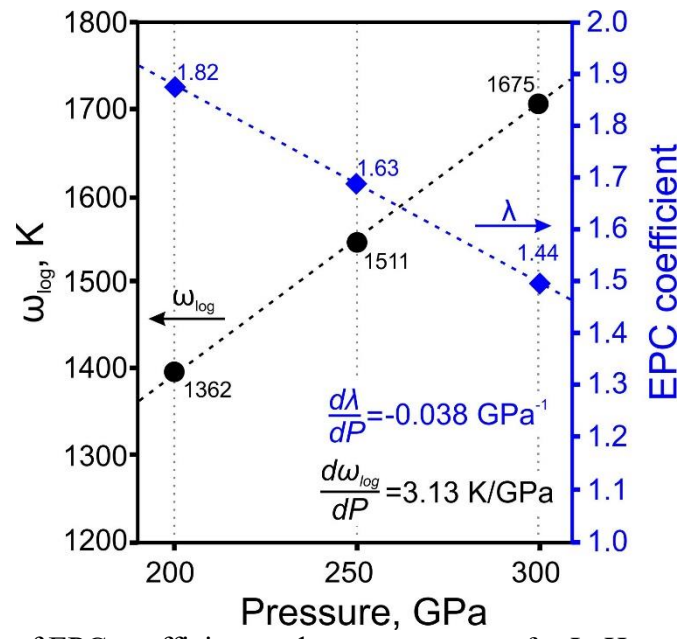


Fig. S19. Dependence of EPC coefficient and ω_{\log} on pressure for LaH₁₆.

Stability of LaH₁₀ polymorphs

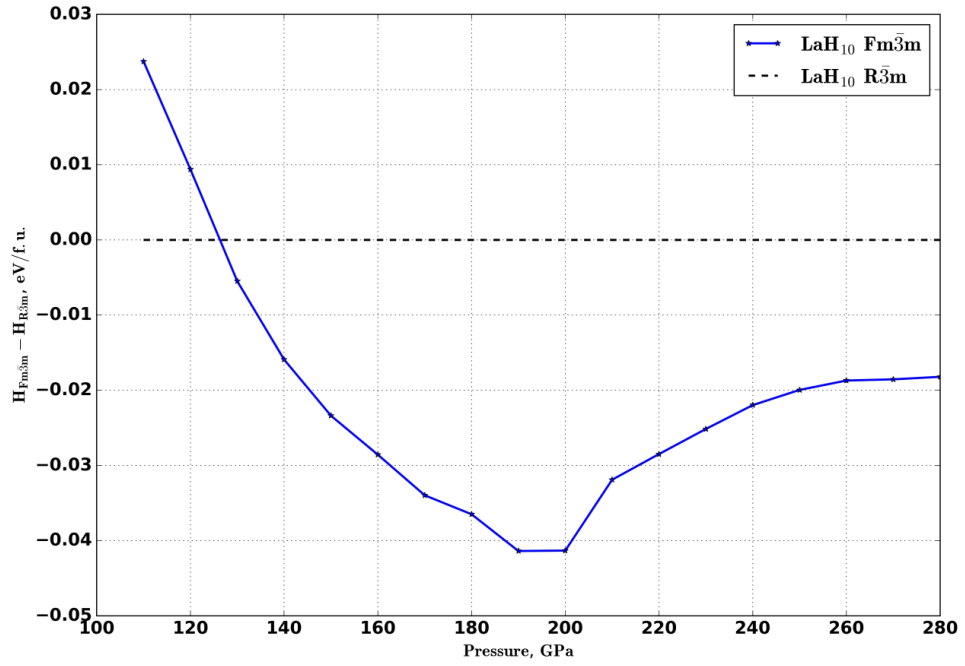


Fig. S20. Enthalpy difference between $Fm\bar{3}m$ -LaH₁₀ and $R\bar{3}m$ -LaH₁₀. Undoubtedly, the transition $Fm\bar{3}m \rightarrow R\bar{3}m$ plays an important role in the measured record superconductivity of LaH₁₀. Such structural transitions accompany superconductivity in H₃S ($C2/c \rightarrow R\bar{3}m \rightarrow Im\bar{3}m$) [24], in Nb₃Al, V₃Ga [25] and in other well-known superconductors.

Matlab functions for T_C calculation using Allen's algorithm from Ref. 10

```

function Solve_Elisahberg(Ef, Tf, mu, filename)
% filename is the name of file with a2F function
N = 24; % dimension of the matrix  $K_{nm}$ 
mu = 0.1; % Coulomb pseudopotential,  $\mu^*$ 
T0 = 1; % initial temperature
Tf = 300; % final temperature
Th = 1; % temperature step
h = 6.626070e-34; % Planck constant
k = 1.380e-23; % Boltzmann constant

t = T0:Th:Tf; % Temperature interval
%%% Read a2F function from file
a2F = load(filename);
wmax = max (a2F(:,1)); % max frequency in Ry
wmin = min (a2F(:,1)); % min frequency in Ry
l = length(a2F); % length of a2F
H = (wmax - wmin)/l; % Ry units

a2F(:,1) = a2F(:,1) * 13.6057 * 2.417e+14; % convert Ry to Hz
%%% a2F(:,1) = a2F(:,1) * 1.0e+12; % convert THz to Hz

T=1;
for j = 1:length(t) % Loop for temperature T=j
T=t(j);
for y = 1:N+1 % sum-function S(x), here we turn to the
function L(z,T) and calculate all the partial sums
S1=0;
for z=1:y
S1 = S1+L(z,T,filename);
end
S(y)=S1;
end

D=0;
for n=1:N+1 % calculation of  $K_{mn}$  matrix in two cycles
for m=1:N+1
if n==m
if m==1
D = 2*(m-1)+1+L(0,T);
else
D=2*(m-1)+1+L(0,T)+2*S(m-1);
end
else
D=0;
end
K(m,n)=L(m-n,T)+L(m+n-1,T)-2*mu-D;
end
end
[A,B]=eig(K); %calculation of eigenvalues
B_max(j) = max(max(B)); % maximum eigenvalue
disp(t(j));
end
B_max = B_max';
plot([T0:Th:Tf],B_max(:,1),'r'); % graph crosses zero at the T = Tc
hold on

function [L] = L(R,T,filename) % Function for electron-electron
interaction
% filename is the name of file with a2F function
N = 24; % dimension of the matrix  $K_{nm}$ 
h = 6.626070e-34; % Planck constant

```

```

k = 1.380e-23;                                % Boltzmann constant

%%Read a2F function from file
a2F = load(filename);
l = length(a2F);                               % length of a2F
a2F(:,1) = a2F(:,1) * 13.6057 * 2.417e+14;    % convert Ry to Hz
%%a2F(:,1) = a2F(:,1) * 1.0e+12;            % convert THz to Hz

Int = 0;
for xx=1:l-1
    Int = Int + (a2F(xx+1,1)-a2F(xx,1)) * 2 * a2F(xx,2) * (h^2) * ...
    a2F(xx,1) / ((h * a2F(xx,1))^2 + (6.283 * (R) * k * T)^2);
end
L=Int;

% It should be noted that the lines a2F = load(filename) in L.m function and
in the main script must be changed simultaneously.

```

References

- [1] M. Lüders, M. A. L. Marques, N. N. Lathiotakis, A. Floris, G. Profeta, L. Fast, A. Continenza, S. Massidda, and E. K. U. Gross, *Phys. Rev. B* **72**, 024545 (2005).
- [2] M. A. L. Marques, M. Lüders, N. N. Lathiotakis, G. Profeta, A. Floris, L. Fast, A. Continenza, E. K. U. Gross, and S. Massidda, *Phys. Rev. B* **72**, 024546 (2005).
- [3] R. Akashi and R. Arita, *Phys. Rev. B* **88**, 014514 (2013).
- [4] R. Akashi, M. Kawamura, S. Tsuneyuki, Y. Nomura, and R. Arita, *Phys. Rev. B* **91**, 224513 (2015).
- [5] D. Pines, *Elementary Excitations in Solids : Lectures on Phonons, Electrons, and Plasmons* (Perseus, Reading, Mass, 1999).
- [6] J. Rath and A. J. Freeman, *Phys. Rev. B* **11**, 2109 (1975).
- [7] P. E. Blöchl, *Phys. Rev. B* **50**, 17953 (1994).
- [8] G. M. Eliashberg, *JETP* **11**, 696 (1959).
- [9] G. Bergmann and D. Rainer, *Z. Für Phys.* **263**, 59 (1973).
- [10] P. B. Allen and R. C. Dynes, Tech. Rep. 7 TCM41974 (1974).
- [11] R. Szczyński, *Acta Phys. Pol. A* **109**, 179 (2006).
- [12] R. Szczyński, *Solid State Commun.* **138**, 347 (2006).
- [13] A. P. Durajski, D. Szczyński, and R. Szczyński, *Solid State Commun.* **200**, 17 (2014).
- [14] K. S. D. Beach, R. J. Gooding, and F. Marsiglio, *Phys. Rev. B* **61**, 5147 (2000).
- [15] J. Bardeen, L. N. Cooper, and J. R. Schrieffer, *Phys. Rev.* **108**, 1175 (1957).
- [16] J. P. Carbotte, *Rev. Mod. Phys.* **62**, 1027 (1990).
- [17] A. P. Drozdov, M. I. Eremets, I. A. Troyan, V. Ksenofontov, and S. I. Shylin, *Nature* **525**, 73 (2015).
- [18] A. P. Drozdov, P. P. Kong, V. S. Minkov, S. P. Besedin, M. A. Kuzovnikov, S. Mozaffari, L. Balicas, F. Balakirev, D. Graf, V. B. Prakapenka, E. Greenberg, D. A. Knyazev, M. Tkacz, and M. I. Eremets, *ArXiv181201561 Cond-Mat* (2018).
- [19] P. B. Allen and R. C. Dynes, *Phys. Rev. B* **12**, 905 (1975).
- [20] H. Liu, I. I. Naumov, R. Hoffmann, N. W. Ashcroft, and R. J. Hemley, *Proc. Natl. Acad. Sci.* **114**, 6990 (2017).
- [21] N. P. Salke, M. M. D. Esfahani, Y. Zhang, I. A. Kruglov, J. Zhou, Y. Wang, E. Greenberg, V. B. Prakapenka, A. R. Oganov, and J.-F. Lin, *ArXiv:1805.02060* <https://arxiv.org/ftp/arxiv/papers/1805/1805.02060.pdf> (2018).
- [22] I. A. Kruglov, A. G. Kvashnin, A. F. Goncharov, A. R. Oganov, S. S. Lobanov, N. Holtgrewe, Sh. Jiang, V. B. Prakapenka, E. Greenberg, and A. V. Yanilkin, *Sci Adv* **4**, eaat9776 (2018).
- [23] D. V. Semenok, I. A. Kruglov, A. G. Kvashnin, and A. R. Oganov, *ArXiv180600865 Cond-Mat* (2018).
- [24] I. Kruglov, R. Akashi, S. Yoshikawa, A. R. Oganov, and M. M. D. Esfahani, *Phys. Rev. B* **96**, 220101 (2017).
- [25] R. Viswanathan, *Mater. Res. Bull.* **9**, 277 (1974).